Reconstruction across imaging modalities: MRI

Brad Sutton

bsutton@Illinois.edu

Bioengineering and Beckman Institute

ILLINOIS

Beckman Institute for Advanced Science & Technology

Introduction to Spins and Classical MRI Physics

Most MRI scans are looking at hydrogen nucleus.

This is good: Body is mostly water ➡ H_2O

Other nuclei are available in MRI:

^{13}C, ^{19}F, ^{23}Na, others

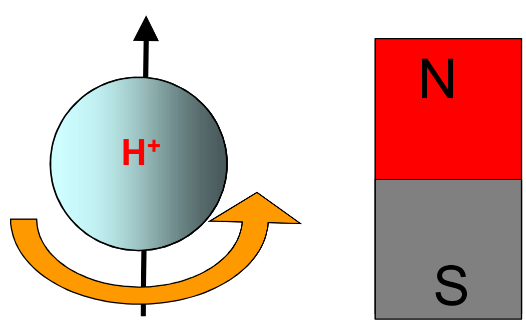

Spinning proton == SPIN

Spinning proton has a magnetic moment ::

Classical Description: Behaves as a bar magnet.

Sample outside the MRI magnet, spins randomly oriented.

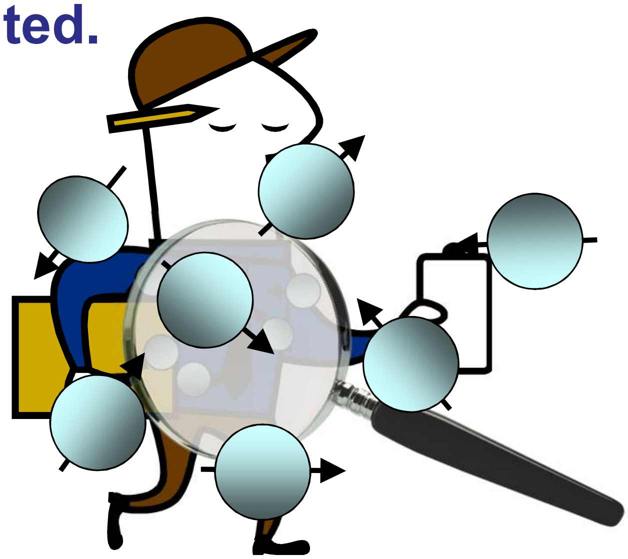

Place sample in the MRI magnet…

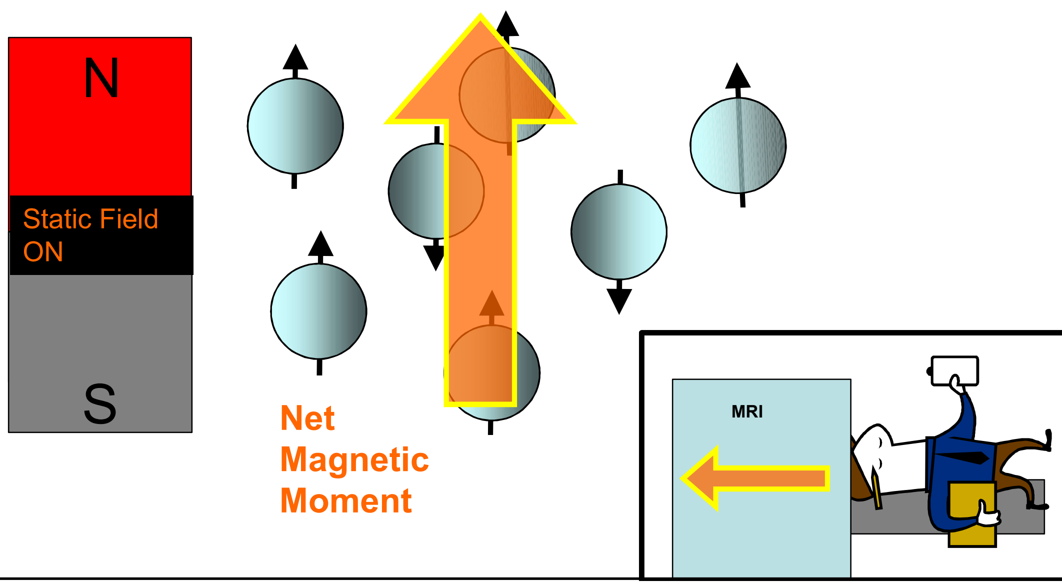

From spins to signal:

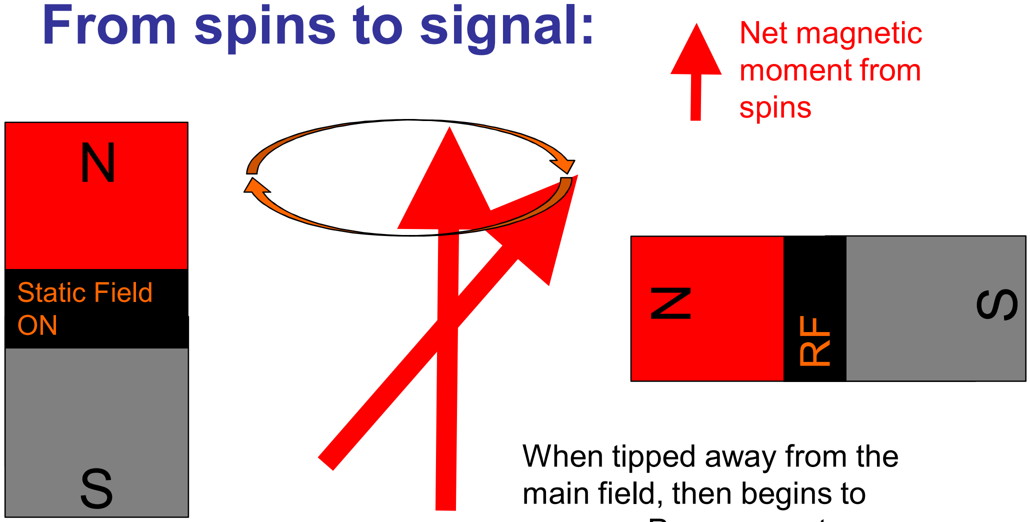

When tipped away from the main field, then begins to precess. Precesses at a frequency proportional to the magnetic field strength. At 3 T = 128 MHz

Localization in Space: Larmor Precession

Since frequency is proportional magnetic field strength if we apply a magnetic field that varies with spatial position, the precession frequency varies with spatial position.

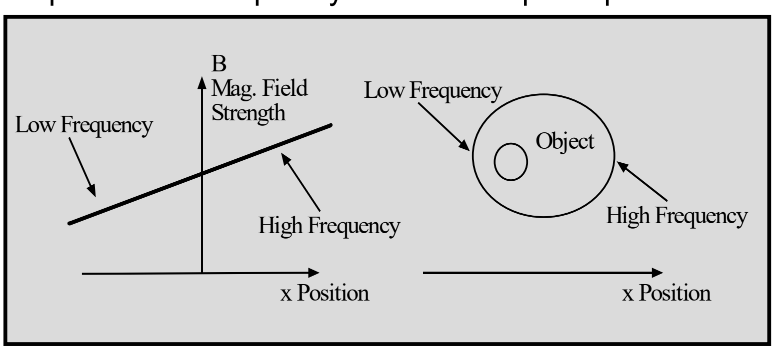

From Noll: fMRI Primer: http://fmri.research.umich.edu/documents/fmri_primer.pdf

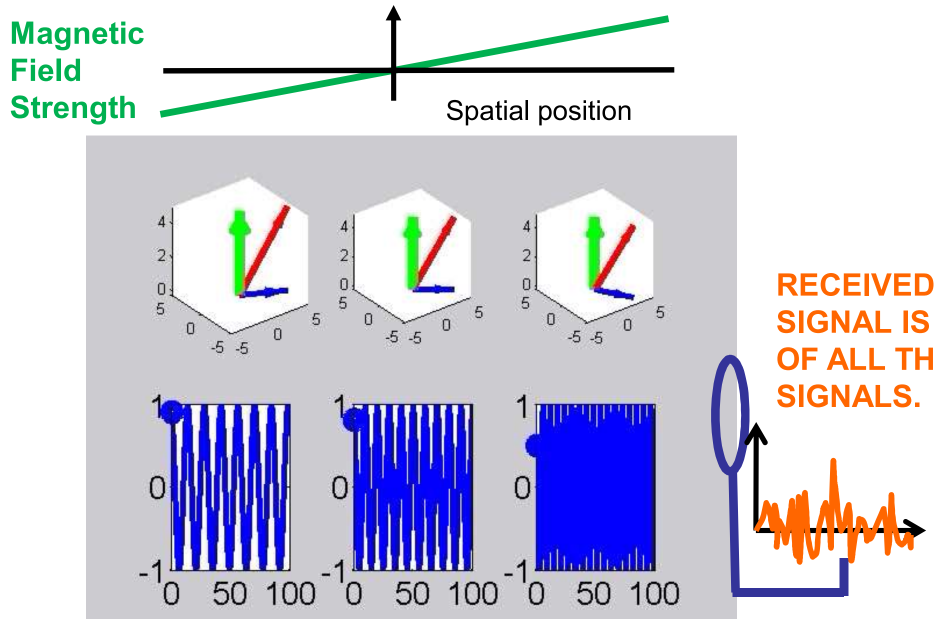

Fourier Image Reconstruction (1D)

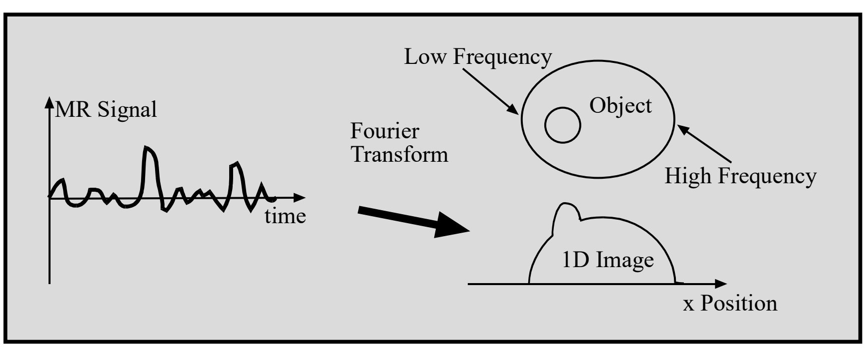

Projection similar to CT!

From Noll: fMRI Primer: http://fmri.research.umich.edu/documents/fmri_primer.pdf

2D Imaging - 2D Fourier Transform

- Fourier encoding also works in 2 and 3 dimensions:

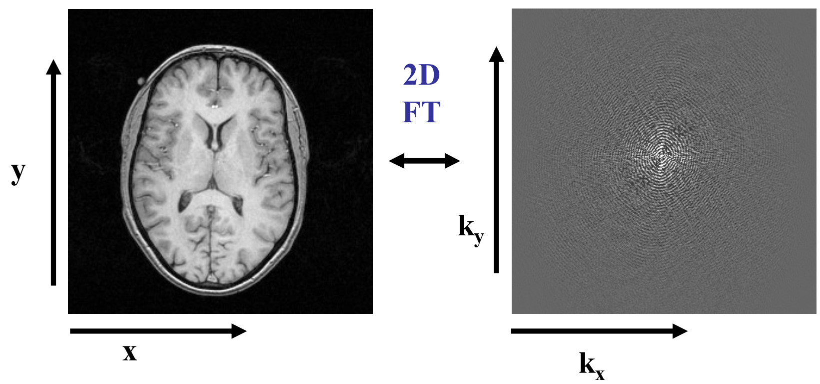

K-space

- We keep track of how much encoding (gradient amplitude times time it is on) by location in k-space:

$$k_x(t) = \bar{\gamma} \int_0^t G_x(\tau) d\tau$$

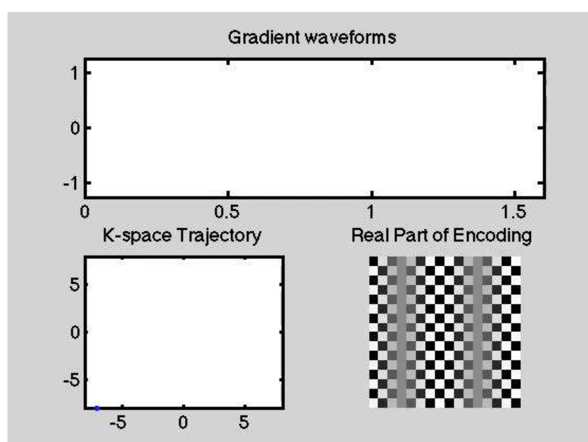

- This is similar to wave number or K-number, it captures the number of spatial cycles of intensity per unit distance
- Fill in k-space, then reconstruction by Fourier Transform

$\bar{\gamma}$ = 42.58 MHz/Tesla

What about non-Cartesian Acquisitions?

- Instead of sampling regular k-space locations on a Cartesian grid, more efficient sampling might include:

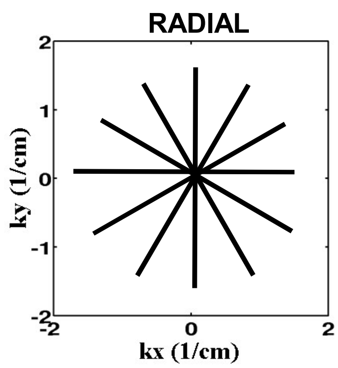

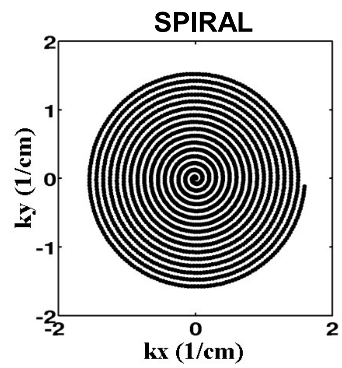

Non-Cartesian: <u>Direct</u> Reconstruction Approach

$$s(\vec{k}) = \int_{FOV} m(\vec{r}) e^{-i2\pi\vec{k}(t)\cdot\vec{r}} d\vec{r}$$

Signal Equation for MRI
NOTE: dr is evenly spaced pixels

- Can perform Inverse Fourier Transform, but must be careful

$$\hat{m}(\vec{r}) = \int_{\vec{k}} s(\vec{k}) e^{i2\pi\vec{k}(t)\cdot\vec{r}} d\vec{k}$$

IFT Reconstruction
NOTE: dk is NOT evenly spaced

- Have to take into account differences in sampling density in different areas of k-space, $d\vec{k}$

Sample Density Compensation

- Density compensation function (DCF) represents the differential area element for each sample.
- Can calculate DCF in many ways:
  - Voronoi area (shown)
  - Analytical formulation of gradient
  - Jacobian of time/k-space transformation
  - PSF optimization

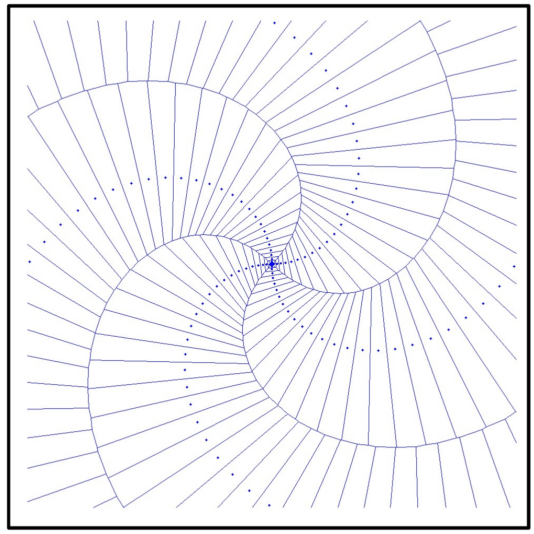

DCF Calculation via Voronoi diagram for 4 shot spiral, showing sampling locations and differential area elements

With DCF, now can perform recon

- Inverse Discrete Space Fourier Transform

$$\hat{m}(\vec{r}) = \sum_j w(\vec{k}_j) s(\vec{k}_j) e^{i2\pi \vec{k}_j \cdot \vec{r}} \qquad w(\vec{k}_j)$$

Density Compensation Function

- But for large problems, we would like to use the Fast Fourier Transform (FFT).
  - **k** is still not equally sampled on regular grid: requirement for FFT!
- What are the options?

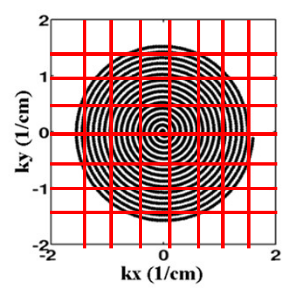

Simply INTERPOLATE onto regular grid and then use FFT?
We will show that we can do better than that with GRIDDING!

Gridding: Fast, accurate, direct recon

- Steps in Gridding
  1. Density compensate k-space data   w(**k**)*s(**k**)
  2. Convolution with a fixed-width blurring kernel to fill in continuous sampling of k-space
  3. Resample data at uniform Cartesian locations
  4. Inverse FFT
  5. Deapodization: Eliminate the effect of the fixed kernel interpolator.

     Convolution in k-space is multiplication in image space, so we can remove the effect of the convolution by dividing by the FT of the kernel in image space.

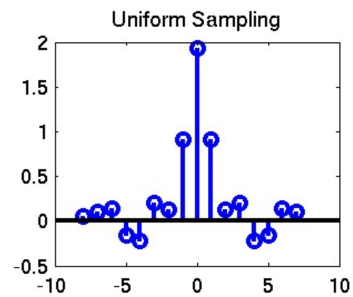

1D simulation from: Noll and Sutton, ISMRM Educational Session, 2003.

Jackson, et al. IEEE Trans Med Imaging. 1991;10(3):473-8.

Gridding is more accurate than interpolation

- 1D Example: Non-uniform spaced samples
- Compared to nearest neighbor interpolation and cubic spline
- Eliminating effect of interpolation drastically increases accuracy!

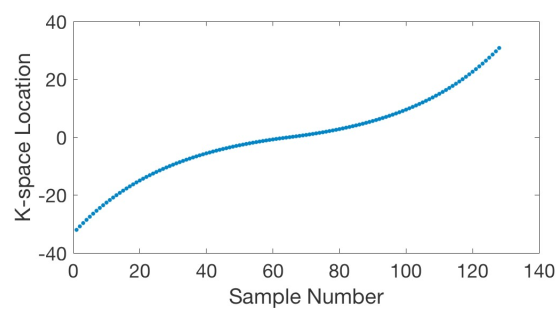

NRMSE:
Nearest: 0.073
Cubic: 0.0143
Gridding: 6.7e-5

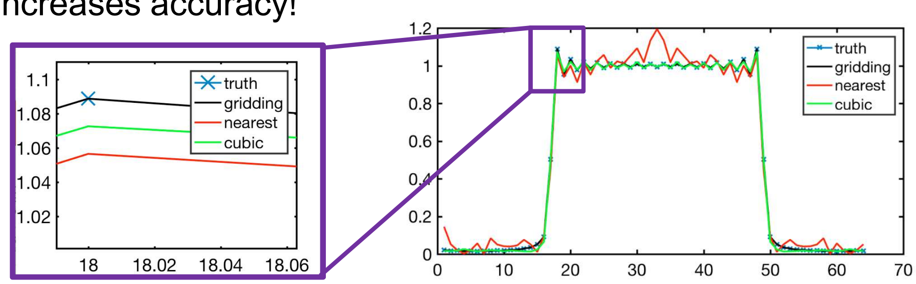

Inverse Problem Approach

Instead of direct inversion, inverse problem approach enables advanced image acquisition and reconstruction

- Variety of additional physics can be accommodated in the signal equation for MRI, enabling advanced acquisitions and reconstructions
  – Coil sensitivities, magnetic field inhomogeneity, k-space trajectory distortions, eddy currents, subject motion, R2* decay, …
- Image regularization penalties can enable faster imaging while making high quality images from fewer samples
  – Total variation, compressed sensing, low rank, …
- Do not need to know sample density compensation function for inverse problem

Signal Model for MRI

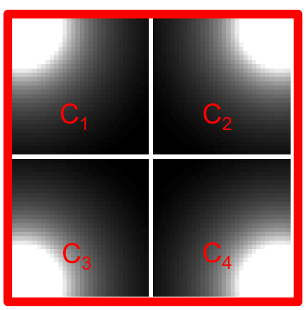

Sensitivity Maps

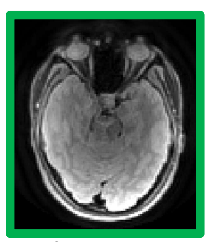
Object

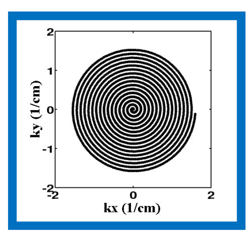

K-space trajectory

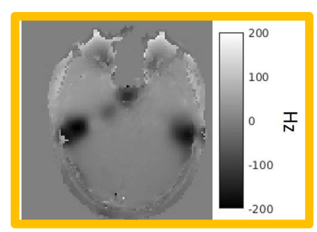

Field Map, ω

$$s_n(\vec{k}_j) = \sum_i \mathrm{sinc}(\vec{k}_j \Delta r) C_n(\vec{r}_i) m(\vec{r}_i) e^{-i2\pi \vec{k}_j \cdot \vec{r}_i} e^{-i\omega(\vec{r}_i) t_j}$$

$$\mathbf{y}_n = \mathbf{s}_n + \epsilon_n = \mathbf{A}\mathbf{C}_n\mathbf{m} + \epsilon_n \quad \Rightarrow \quad \mathbf{y} = \mathcal{A}\mathbf{m} + \epsilon$$

Inverse problem approach

- In complex-valued MRI, noise is complex Gaussian.
- Makes statistics easier than other modalities
- Can use least squares approaches for image reconstruction $$\hat{\mathbf{m}} = \arg\min_{\mathbf{m}} \|\mathbf{y} - \mathbf{A}\mathbf{m}\|_2^2$$
- Can add regularization to help with the usually ill-conditioned problem, provides prior information on acceptable solutions, through some function $\mathcal{R}()$

$$\hat{\mathbf{m}} = \arg\min_{\mathbf{m}} \|\mathbf{y} - \mathbf{A}\mathbf{m}\|_2^2 + \lambda\mathcal{R}(\mathbf{m})$$

Example: Magnetic Field Inhomogeneity

Incorporation of the field inhomogeneity map into the inverse problem to correct for it.

Air/tissue interfaces cause most magnetic field disruptions, for example around sinuses.

B_0 *(ppm)*

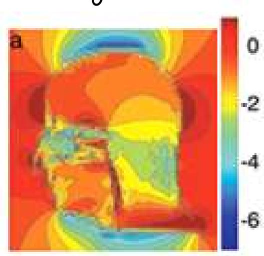

Air/Tissue interfaces can cause up to ~1 KHz off-resonance at 3 T

Image Distortion

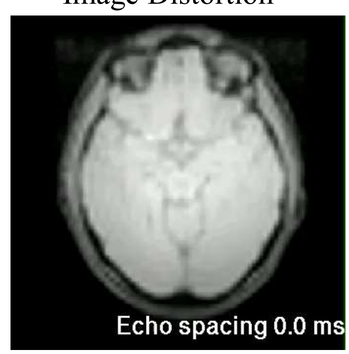

Distortion depends on K-space trajectory and bandwidth (how fast sample k-space).

Example: Magnetic Field Inhomogeneity

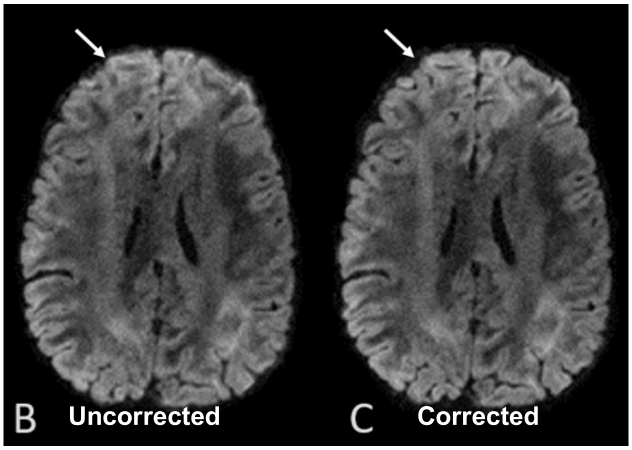

High Resolution (0.8 mm isotropic) diffusion MRI, b=1000 s/mm^2

Dynamic Speech Imaging with FLASH. Air/tissue susceptibility can be 1.2 kHz at 3 T.

Uncorrected Corrected Field Map

Holtrop and Sutton. J Medical imaging. 3(2): 023501 (2016).
Sutton, et al. J Magn Reson Imaging. 32:1228 (2010)

Regularization and Constraints

- Image reconstruction is ill-conditioned problem
  - Sample only the minimum data (or less) that we need to keep scan time short
  - Push the spatial resolution higher → signal-to-noise lower
  - Non-ideal experimental conditions
    - Magnetic field map changed since measurement
    - Coil sensitivies changed
    - K-space trajectory deviations
- Must enforce prior information on the solution in order to achieve a high quality image

Types of Regularization/Constraints in MRI

- Not an exhaustive list, just main ones
- Energy penalty, reference image, Tikhonov
- Roughness penalty, first order derivative,
- TV - total variation
- Compressed sensing
  - Sparsity, Finite differences, DCT, Wavelets, … thresholding

- Something to keep in mind: MRI images are complex valued – have magnitude and phase

Compressed Sensing

- CS takes advantage of k-space sampling patterns that cause **incoherent aliasing** from the undersampling.
  - Distributes aliasing energy around in an incoherent manner
  - Makes it noise-like
- Transforms images into a domain where they are **sparse**
- **Recovers sparse coefficients** in the background noise of aliasing – similar to denoising algorithms

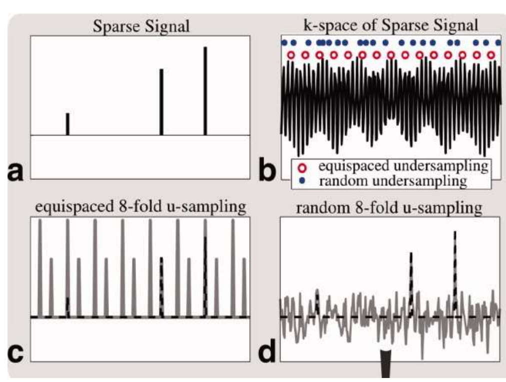

Figure from: Lustig, Donoho, Pauly. Magn Reson Med, 58:1182 (2007)

https://people.eecs.berkeley.edu/~mlustig/CS.html

Low Rank through Partial Separability

- Not only are images typically sparse in finite difference or wavelet domains, dynamic timeseries data are typically low rank
- Low rank indicates strong spatial-temporal correlations in the data set.

- Simple example to play around with at:

http://go.illinois.edu/LowRank

Partial Separability (PS) Model

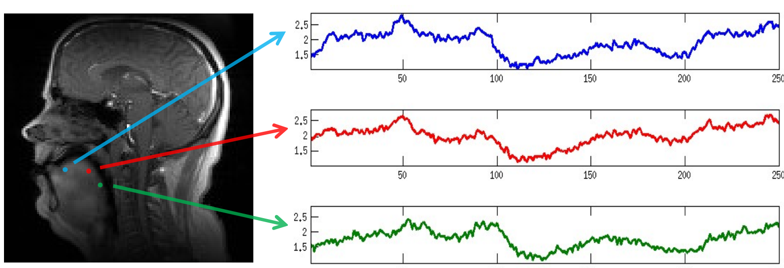

/loo/ - /lee/ - /la/ sounds
100 frames per second

- Leverages strong spatiotemporal correlation
- L^{th} order Partial Separability model:

$$d(\boldsymbol{k}, t) = \sum_{l=1}^{L} c_l(\boldsymbol{k}) \varphi_l(t)$$

Z.-P. Liang, *IEEE-ISBI*, 2007.

Partial Separability Model

$$s(\mathbf{k},t) = \sum_{l=1}^{L} c_l(\mathbf{k})\phi_l(t) \Rightarrow \mathbf{C} = \begin{bmatrix} s(\mathbf{k}_1,t_1) & s(\mathbf{k}_1,t_2) & \cdots & s(\mathbf{k}_1,t_M) \\ s(\mathbf{k}_2,t_1) & s(\mathbf{k}_2,t_2) & \cdots & s(\mathbf{k}_2,t_M) \\ \vdots & \vdots & & \vdots \\ s(\mathbf{k}_N,t_1) & s(\mathbf{k}_N,t_2) & \cdots & s(\mathbf{k}_N,t_M) \end{bmatrix}$$

Spatial Bases ($c_l(\mathbf{k})$) — Temporal Bases ($\phi_l(t)$)

$\mathrm{rank}(C) \le L$, over any point set $\{(\mathbf{k}_m, t_n)\}_{m,n=1}^{M,N}$

$$\mathbf{C} = \begin{pmatrix} s(\mathbf{k}_1,t_1) & ? & \cdots & s(\mathbf{k}_1,t_p) & ? & \cdots & ? & s(\mathbf{k}_1,t_m) \\ ? & s(\mathbf{k}_2,t_2) & ? & \cdots ? & s(\mathbf{k}_2,t_q) & \cdots & ? & ? \\ & & \cdots & & & & & \\ s(\mathbf{k}_n,t_1) & ? & ? \cdots & s(\mathbf{k}_n,t_l) & & \cdots & ? & s(\mathbf{k}_n,t_m) \end{pmatrix}$$

$$\hat{\mathbf{C}} = \arg\min_{\hat{\mathbf{C}}} \| \boldsymbol{\Pi}(\mathbf{C} - \hat{\mathbf{C}}) \|_2^2 \quad \text{s.t.} \quad \mathrm{rank}(\hat{\mathbf{C}}) = L$$

$$\hat{\mathbf{C}} = \arg\min_{\hat{\mathbf{C}}} \| \boldsymbol{\Pi}(\mathbf{C} - \hat{\mathbf{C}}) \|_2^2 + \lambda \| \hat{\mathbf{C}} \|_*$$

Z.-P. Liang, *IEEE-ISBI*, 2007.

Partial Separability Model

$$\mathbf{C} = \begin{pmatrix} s(\mathbf{k}_1,t_1) & ? & \cdots & s(\mathbf{k}_1,t_i) & ? & \cdots & ? & \cdots & s(\mathbf{k}_1,t_m) \\ ? & s(\mathbf{k}_2,t_2) & ? & \cdots & ? & s(\mathbf{k}_2,t_j) & \cdots & ? & ? \\ & & \cdots & & & & & & \\ & & \cdots & & & & & & \\ \hat{s}(\mathbf{k}_p,t_1) & \hat{s}(\mathbf{k}_p,t_2) & \cdots & \hat{s}(\mathbf{k}_p,t_i) & \cdots & \hat{s}(\mathbf{k}_p,t_j) & \cdots & \hat{s}(\mathbf{k}_p,t_{m-1}) & \hat{s}(\mathbf{k}_p,t_m) \\ \hat{s}(\mathbf{k}_{p+1},t_1) & \hat{s}(\mathbf{k}_{p+1},t_2) & \cdots & \hat{s}(\mathbf{k}_{p+1},t_i) & \cdots & \hat{s}(\mathbf{k}_{p+1},t_j) & \cdots & \hat{s}(\mathbf{k}_{p+1},t_{m-1}) & \hat{s}(\mathbf{k}_{p+1},t_m) \\ \hat{s}(\mathbf{k}_{p+q},t_1) & \hat{s}(\mathbf{k}_{p+q},t_2) & \cdots & \hat{s}(\mathbf{k}_{p+q},t_i) & \cdots & \hat{s}(\mathbf{k}_{p+q},t_j) & \cdots & \hat{s}(\mathbf{k}_{p+q},t_{m-1}) & \hat{s}(\mathbf{k}_{p+q},t_m) \\ & & \cdots & & & & & & \\ & & \cdots & & & & & & \\ s(\mathbf{k}_n,t_1) & ? & ? & \cdots & \cdots & \cdots & s(\mathbf{k}_n,t_l) & ? & s(\mathbf{k}_n,t_m) \end{pmatrix}$$

Navigator Data
- High temporal sampling speed
- Limited **k**-space locations
- Determines $\{\phi_l(t)\}_{l=1}^{L}$

Imaging Data
- Extended **k**-space locations
- Low temporal sampling speed
- Determines $\{c_l(\mathbf{k})\}_{l=1}^{L}$

28

Z.-P. Liang, *IEEE-ISBI*, 2007.

PS Model-based Image Reconstruction

- Step 1: determination of temporal basis functions

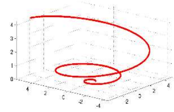

$$\begin{bmatrix} d_1(\boldsymbol{k}_1,t_1) & d_1(\boldsymbol{k}_2,t_1) & \cdots & d_1(\boldsymbol{k}_N,t_1) \\ d_1(\boldsymbol{k}_1,t_2) & d_1(\boldsymbol{k}_2,t_2) & \cdots & d_1(\boldsymbol{k}_N,t_2) \\ \vdots & \vdots & \ddots & \vdots \\ d_1(\boldsymbol{k}_1,t_M) & d_1(\boldsymbol{k}_2,t_M) & \cdots & d_1(\boldsymbol{k}_N,t_M) \end{bmatrix} = \sum_{l=1}^{L} \lambda_l \boldsymbol{u}_l \boldsymbol{v}_l^H$$

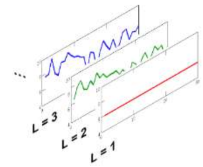

$\{\varphi_l(t)\}_{l=1}^{L}$

- Step 2: estimation of spatial basis functions

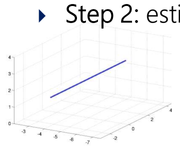

$$\{\hat{c}_l(\boldsymbol{k})\}_{l=1}^{L} = \arg\min_{\{c_l(\boldsymbol{k})\}_{l=1}^{L}} \left\| d_2(\boldsymbol{k},t) - \boldsymbol{E}\left\{\sum_{l=1}^{L} c_l(\boldsymbol{k})\varphi_l(t)\right\} \right\|_2^2$$

$\{C_l(\boldsymbol{r})\}_{l=1}^{L}$

- Step 3: synthesis of $(k,\ t)$-space / $(x,\ t)$-space data

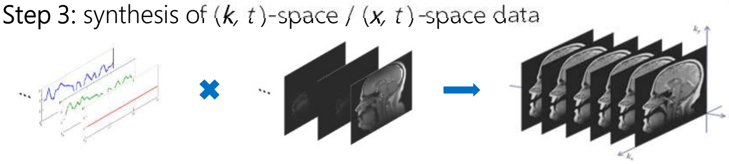

Fu et al, Magn Reson Med, 2015, 2017

PS-Sparse Reconstruction

- Jointly enforcing the partial separability constraint and the spatial-spectral sparsity constraint

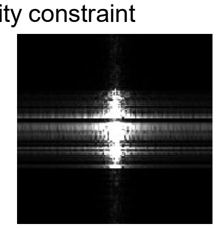

$(x,\ f)$ - spectrum

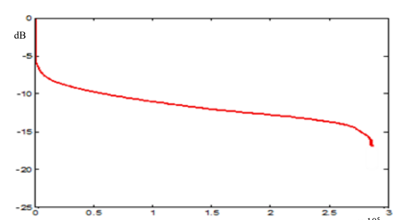

Sorted $(x,\ f)$ - coefficients

- Formulation: $$\{\hat{c}_l(\boldsymbol{k})\}_{l=1}^{L} = \arg\min_{\{c_l(\boldsymbol{k})\}_{l=1}^{L}} \underbrace{\left\| d_2(\boldsymbol{k},t) - \boldsymbol{E}\left\{\sum_{l=1}^{L} c_l(\boldsymbol{k})\varphi_l(t)\right\} \right\|_2^2}_{\text{Data consistency constraint}} + \lambda \underbrace{\left\| \boldsymbol{F}_{k,t}\left\{\sum_{l=1}^{L} c_l(\boldsymbol{k})\varphi_l(t)\right\} \right\|_1}_{\text{Spatial-spectral sparsity constraint}}$$
- An algorithm based on half-quadratic regularization has been proposed to solve this optimization problem [1].

[1] B. Zhao *et al*, *TMI,* 2012.

What you can achieve with PS-Sparse

Subject:
A female speaker of Mid-Atlantic American English
Spatial coverage:
$280 \times 280 \times 40$ mm^3
Matrix size:
$128 \times 128 \times 8$
Spatial resolution:
$2.2 \times 2.2 \times 5.0$ mm^3
Nominal Frame Rate:
166 frames per second!

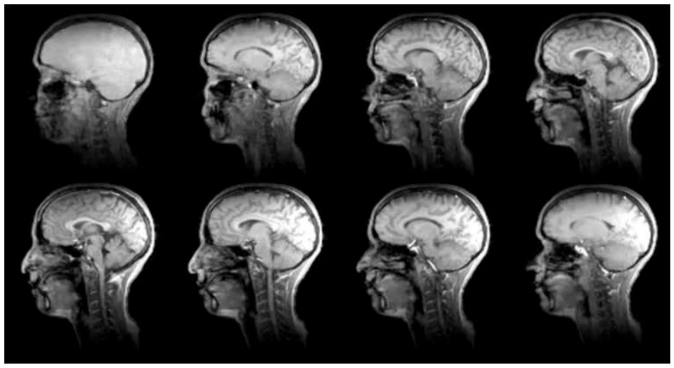

Carrier Phrase – "I said writing to you, I said riding to you" [1]

Fu, Barlaz, Holtrop, et al. Magn Reson Med 77(4): 1619, 2017. M. Barlaz et al, InterSpeech, 2015.

Speeding Up Acquisitions: Parallel Imaging

- Reconstruction approaches above did not leverage the use of multiple, smaller receiver coils
- Each coil is most sensitive to tissue in its local area
- Reduced spatial encoding requirements because aliasing signal may overlap region where there is low sensitivity for a coil
- Easily incorporated into cost function for sensitivity encoding (SENSE)

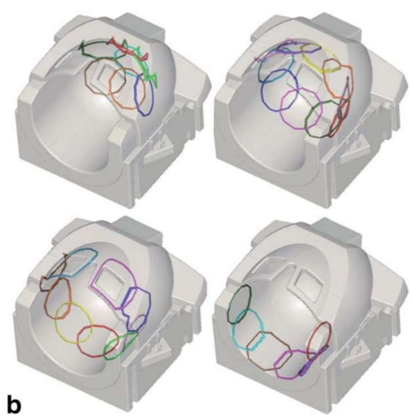

Kaza, Klose, and Lotze. J Magn Reson Imaging. 34:173 (2011)

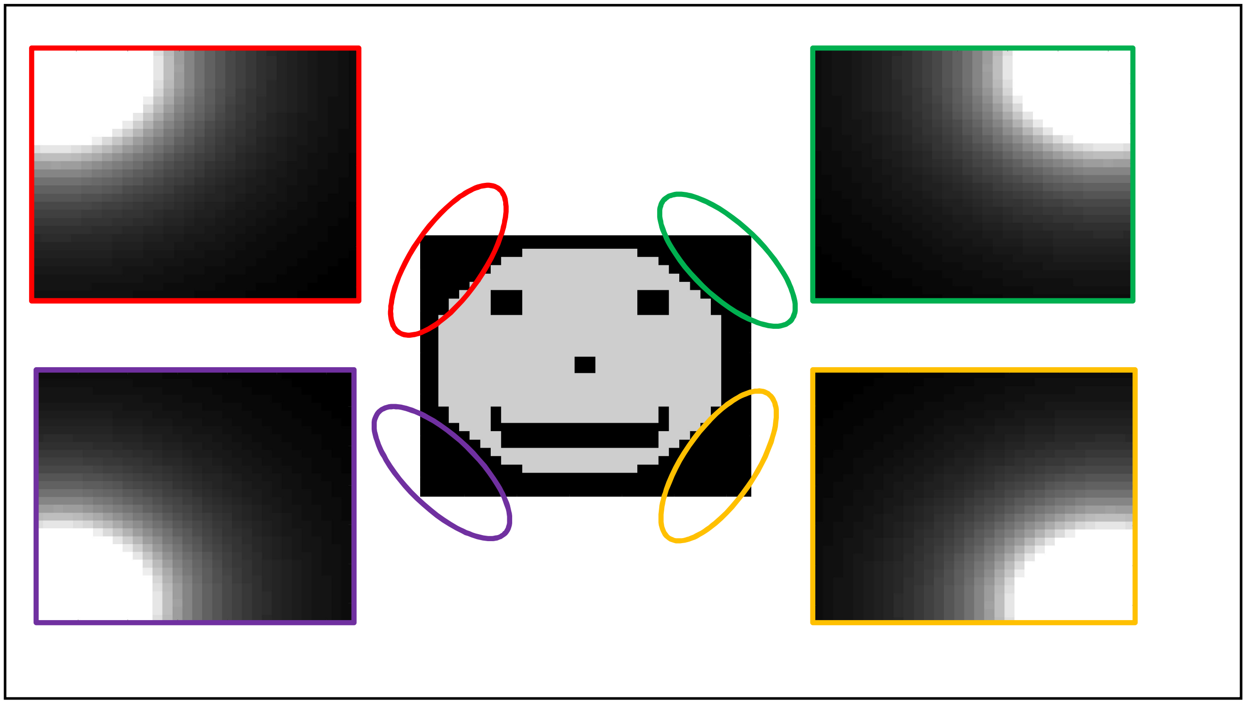

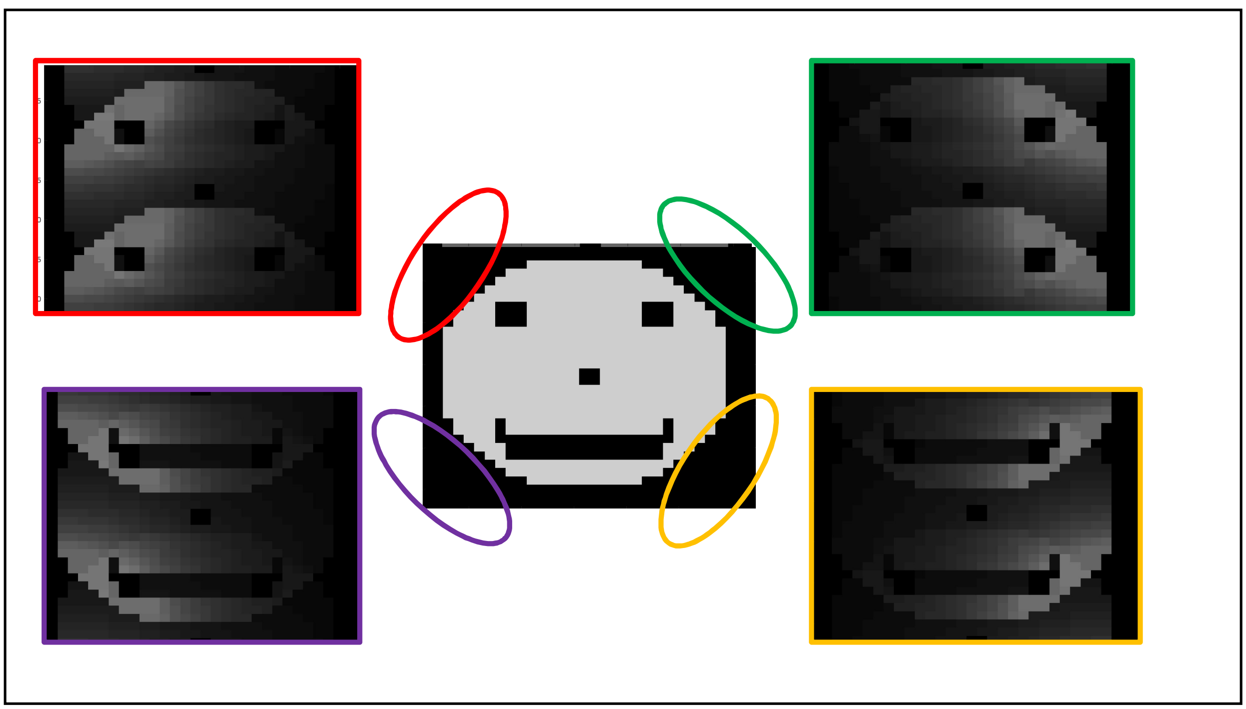

Parallel Imaging Reconstruction

- SENSE – least squares estimation with coil sensitivities in <u>image space</u>

$$s_n(\vec{k}_j) = \sum_i \mathrm{sinc}(\vec{k}_j \Delta r) C_n(\vec{r}_i) m(\vec{r}_i) e^{-i2\pi \vec{k}_j \cdot \vec{r}_i} e^{-i\omega(\vec{r}_i) t_j}$$

- GRAPPA – operates in <u>k-space</u>. Multiplication by coil sensitivities in image space is convolution in k-space. So, find the convolution kernel in k-space to fill in missing samples

Pruessmann, et al. Magn reson Med 42:952 (1999). Griswold, et al. Magn Reson Med 47: 1202 (2002)

GeneRalized Autocalibrating Partially Parallel Acquisitions (GRAPPA)

- Learn linear relationship between kernels of sampled points in k-space to ”interpolate” those that were not sampled.

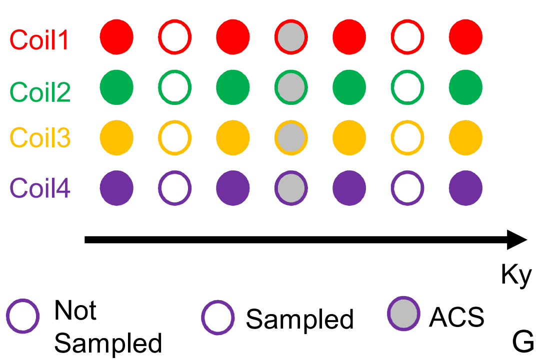

Griswold, et al. Magn Reson Med 47: 1202 (2002)

GeneRalized Autocalibrating Partially Parallel Acquisitions (GRAPPA)

- Learn linear relationship between kernels of sampled points in k-space to ”interpolate” those that were not sampled.

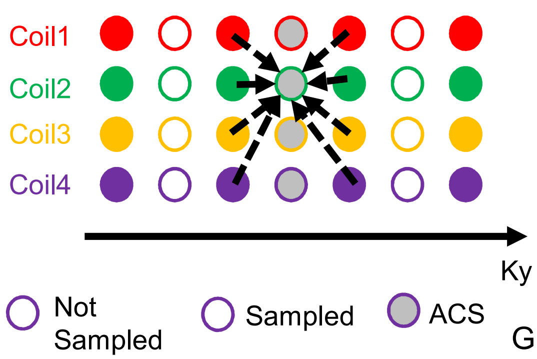

Using Autocalibration points, find the weights required to fit the target point, using adjacent samples from across all coils.

Griswold, et al. Magn Reson Med 47: 1202 (2002)

GeneRalized Autocalibrating Partially Parallel Acquisitions (GRAPPA)

- Learn linear relationship between kernels of sampled points in k-space to ”interpolate” those that were not sampled.

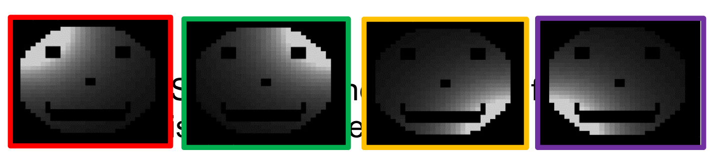

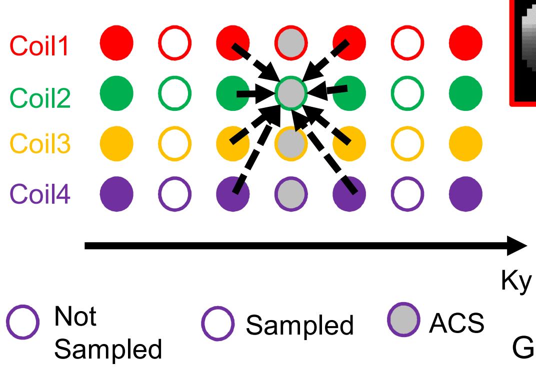

Once k-space filled in – simply Fourier Transform to make an image from EACH COIL.

Griswold, et al. Magn Reson Med 47: 1202 (2002)

COMPUTATIONAL Challenge of Image Reconstruction

- Large matrix size
  - 1.25 mm isotropic data set
- Data Size:
  - 18 GB for 6.5 min scan
- Physics:
  - 3D non-Cartesian (Spiral) sampling
  - Parallel Imaging with 32 channel coil
  - Magnetic Field Inhomogeneity Correction
  - Motion-induced Phase Correction
- Reconstruction Time
  - 8 days for reconstruction running on workstation
- Graphics Processing Units (GPU)
  - 200 times faster: <1 hour.
  - Enables imaging resolutions not feasible before.

GTX 1080 Ti: ~$700 (11 GB)
CORES: 3584
Boost Clock: 1582 MHz

IMPATIENT MRI:
Illinois Massively Parallel Acceleration Toolkit for Image reconstruction with ENhanced Throughput in MRI

PowerGrid –ISMRM 2016, p. 525

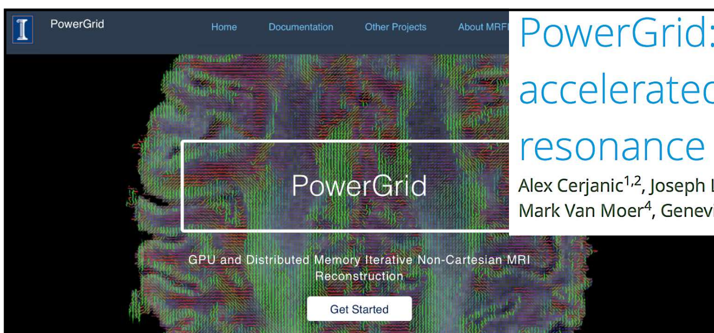

PowerGrid: A open source library for accelerated iterative magnetic resonance image reconstruction

Alex Cerjanic[1,2], Joseph L Holtrop[1,2], Giang Chau Ngo[1], Brent Leback[3], Galen Arnold[4], Mark Van Moer[4], Genevieve LaBelle[2,5], Jeffrey A Fessler[6], and Bradley P Sutton[1,2]

ISMRM 2016, p. 525

http://mrfil.github.io/PowerGrid/

- Enable leveraging of GPU and MPI in MRI reconstructions
- Using ISMRM RD – raw data format standard
- Translating MATLAB routines from IRT into C++ through Armadillo
- Packaging for easy use (Docker) – coming soon

Scale with PowerGrid

- How to use > 1 GPU?
- Message Passing Interface (MPI)
- Phase Corrected SENSE (pcSENSE) for Diffusion Imaging
  - 120 x 120 x 4 x 32 coils

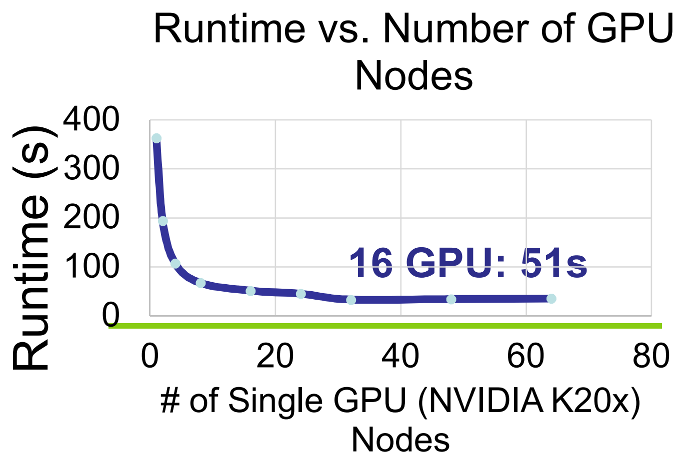

Liu C, Moseley ME, Bammer R. Simultaneous phase correction and SENSE reconstruction for navigated multi-shot DWI with non-cartesian k-space sampling. MRM. 2005;54(6):1412–1422.

K20x: 2688 cores, 732 MHz clock rate. 6 GB.

Push for Free, Open Source, Common Platforms for Image Reconstruction

- Advanced reconstructions are more complex than Fourier Transform, but enable significantly higher resolutions and shorter scan times.
- Image reconstructions can be specific for the sequence, MRI vendor platform, image reconstruction hardware, and can be difficult to reimplement from paper
- There is a growing effort at creating broad-based utilities to enable reproducibility, distribution, scaling, and impact
- Just a few listed here…

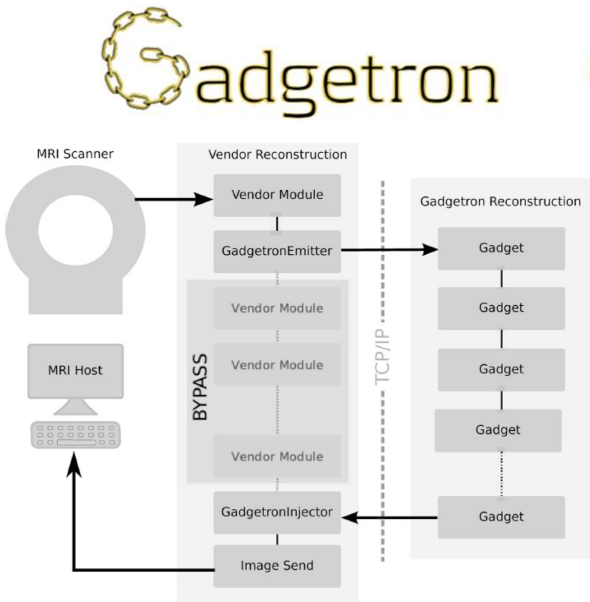

Hansen and Sorensen. Gadgetron. Magn Reson Medicine 69: 1768 (2013)

Michigan Image Reconstruction Toolbox (MIRT)

https://web.eecs.umich.edu/~fessler/code/index.html

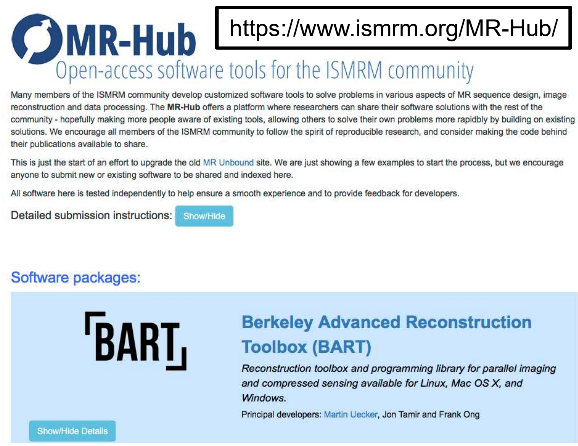

Summary

- Inverse problem approach to MRI reconstruction enables higher resolution, improved SNR, accommodating non-ideal physics for improved image quality
- Comes at a great deal of computational expense (MRI scanner does an efficient job for FFT on Cartesian data)
- Lots of open source powerful code available to translate techniques to clinical research workflows, leveraging clusters and GPU’s
  - TRY THEM OUT!

Quantitative Reconstruction in PET / CT and PET / MR

Georges El Fakhri, PhD, DABR
Gordon Center for Medical Imaging
Massachusetts General Hospital
Harvard Medical School

MASSACHUSETTS GENERAL HOSPITAL
Gordon Center for Medical Imaging
HARVARD MEDICAL SCHOOL

Outline

- PET 101
- Tomography in medical imaging
- Projection imaging
- Sinogram
- Reconstruction-analytic
- Backprojection artifacts
- Reconstruction-iterative
- Comparison of analytic and iterative reconstructions
- Simultaneous PET-MR

Gordon Center for Medical Imaging

History of PET at MGH

The birthplace of Positron Emission Imaging was at MGH in 1952 in the Center for Radiological Sciences (Ancestor of the Gordon Center for Medical Imaging) where the first positron-imaging device was invented by Dr Gordon Brownell and used for the detection of brain tumors for neurosurgery by Dr Sweet (1953)

Coincidence (a) and "unbalance" (b) scans of a patient with recurring tumor (left) under previous operation site [Brownell and Sweet, 1953]

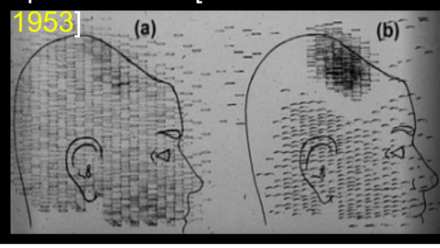

Gordon Center for Medical Imaging

What is tomography?

- Greek translation:
  - *tomos* means slice, section
  - *graph* means write
- 2-D representations of structures in a selected plane of a 3-D object
- Mathematical algorithms can be used to reconstruct the original 3-D object from the 2-D projections
- Used in medical imaging
  - SPECT and PET-Emission computed tomography
  - CT-Transmission computed tomography

http://science.howstuffworks.com/cat-scan1.htm

MGH 1811

Gordon Center for Medical Imaging

History of PET at MGH

MGH is also the birthplace of filtered backprojection that is stil widely used in PET and in CT. Dr David Chesler (Brownell Lab) presented the first results about filtered backprojection at the Meeting of Tomographic Imaging in Nuclear Medicine (1972).

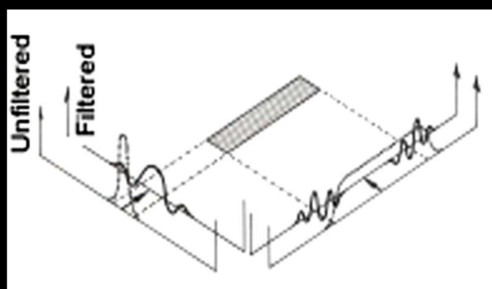

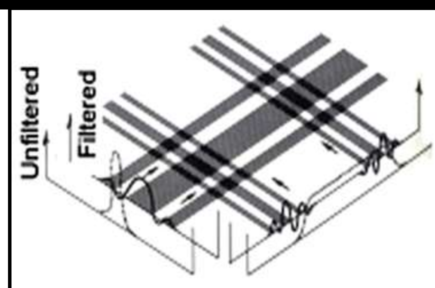

So the PE & T of PET started at MGH!

Gordon Center for Medical Imaging

History

J. Radon

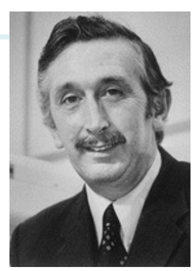

G.N.Hounsfield

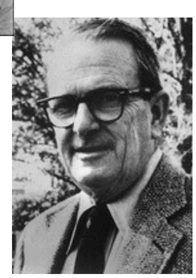

A.M.Cormack

Gordon Center for Medical Imaging

Why tomography over planar imaging?

10	10	10	30
10	20	10	40
10	10	10	30

Contrast (Planar) = (40 – 30)/30 = 0.33
Contrast (Tomo) = (20 – 10)/10 = 1.00

Tomography in medical imaging

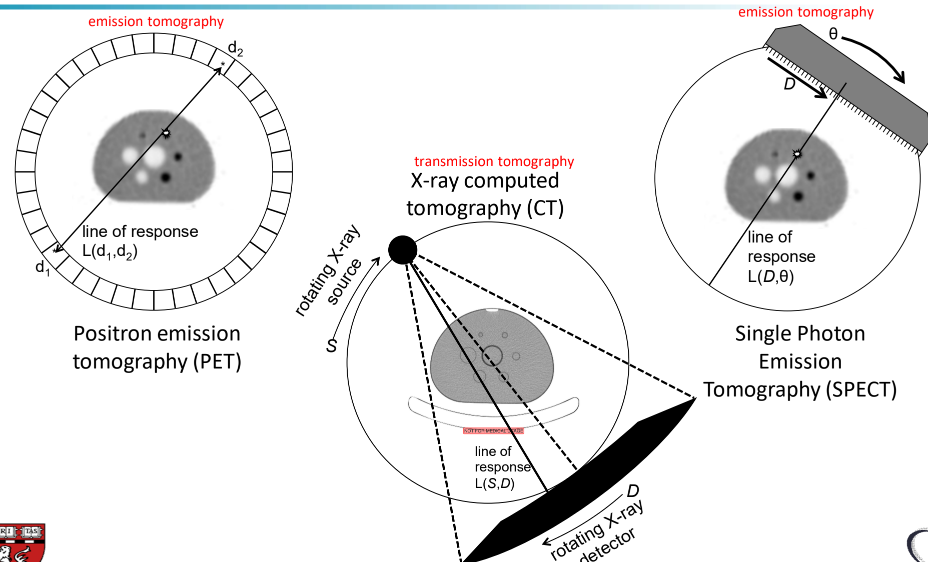

Gamma Ray Emission

Unstable parent nucleus

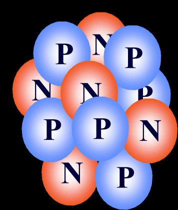

Gamma Ray Emission

Nucleus drops to lower energy state.

Gamma ray carries away excess energy

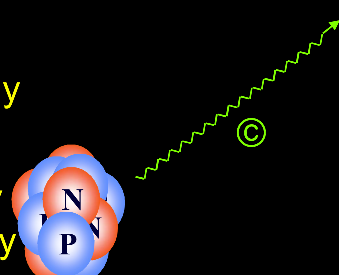

Gamma Ray Emission

Nucleus drops to lower energy state.

Gamma ray carries away excess energy

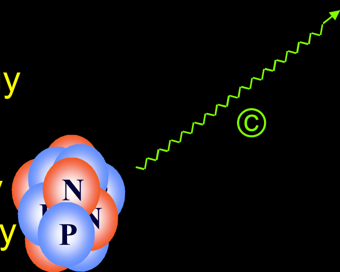

Positron Emission and Annihilation

Unstable parent nucleus with extra proton

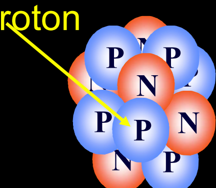

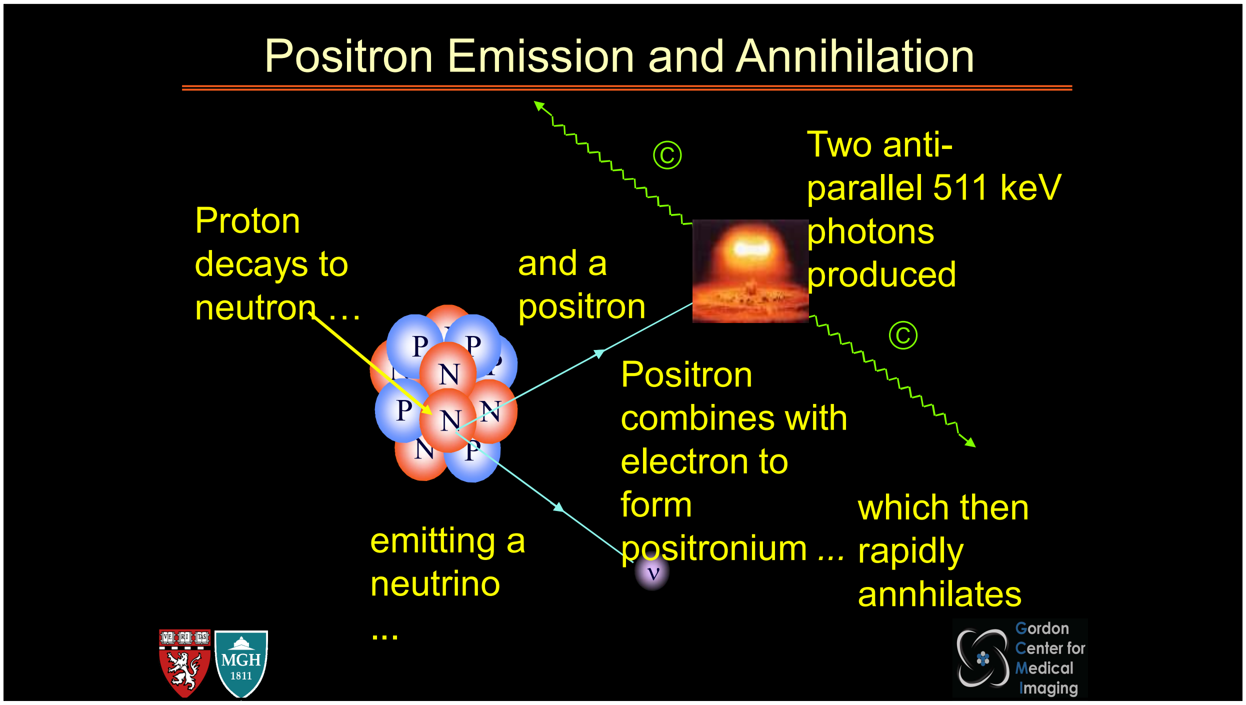
Positron Emission and Annihilation
Proton decays to neutron …
and a positron
emitting a neutrino …
Positron combines with electron to form positronium …
Two anti-parallel 511 keV photons produced
which then rapidly annhilates
Gordon Center for Medical Imaging

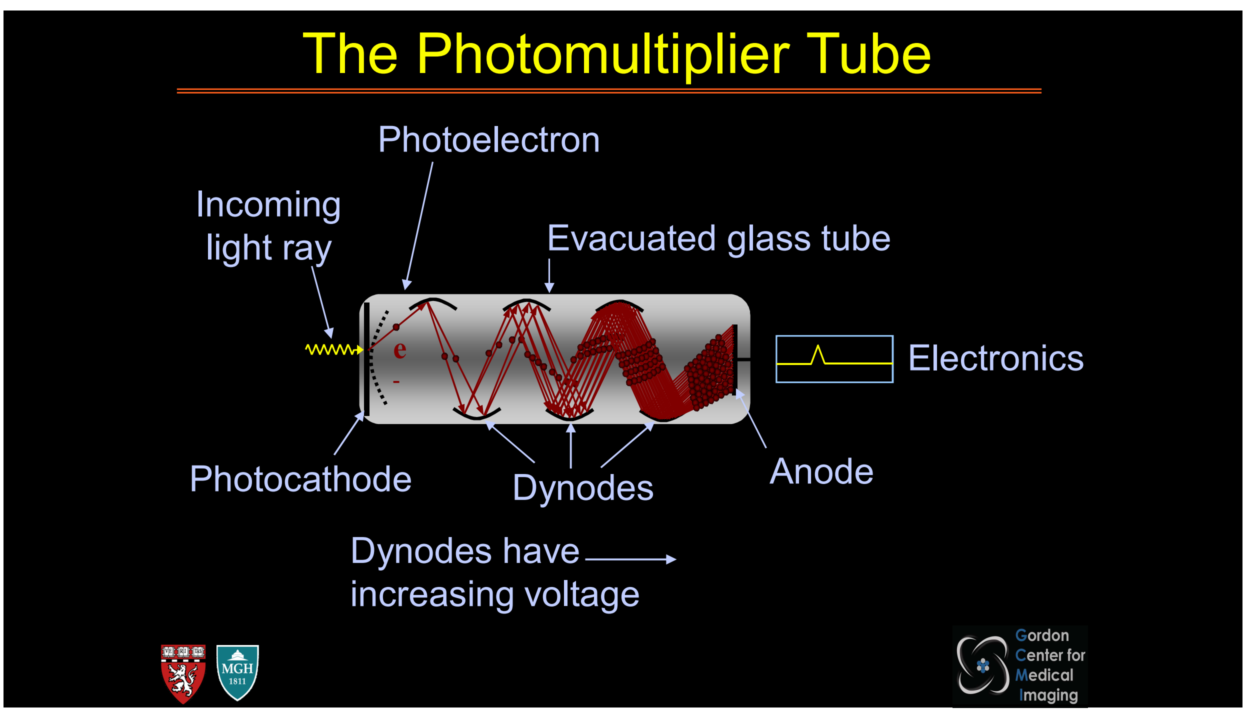
The Photomultiplier Tube
Photoelectron
Incoming light ray
Evacuated glass tube
Electronics
Photocathode
Dynodes
Anode
Dynodes have increasing voltage
Gordon Center for Medical Imaging

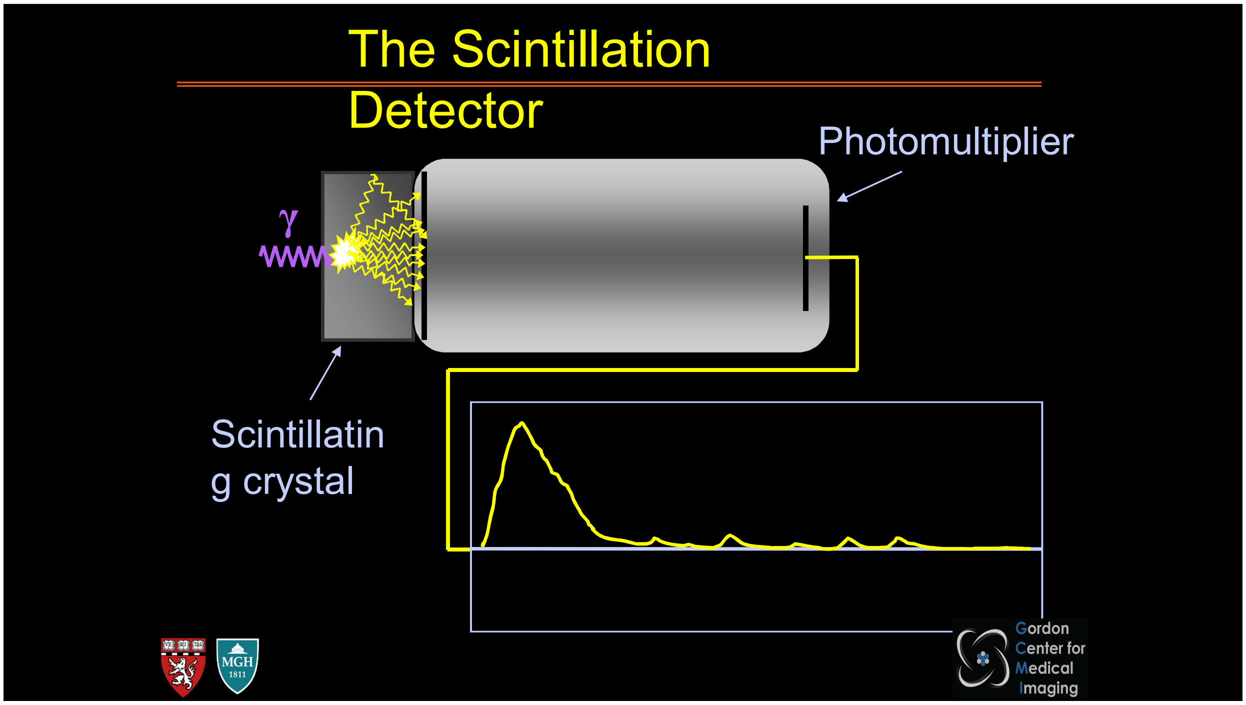
The Scintillation Detector
Photomultiplier
γ
Scintillating crystal
Gordon Center for Medical Imaging
MGH 1811

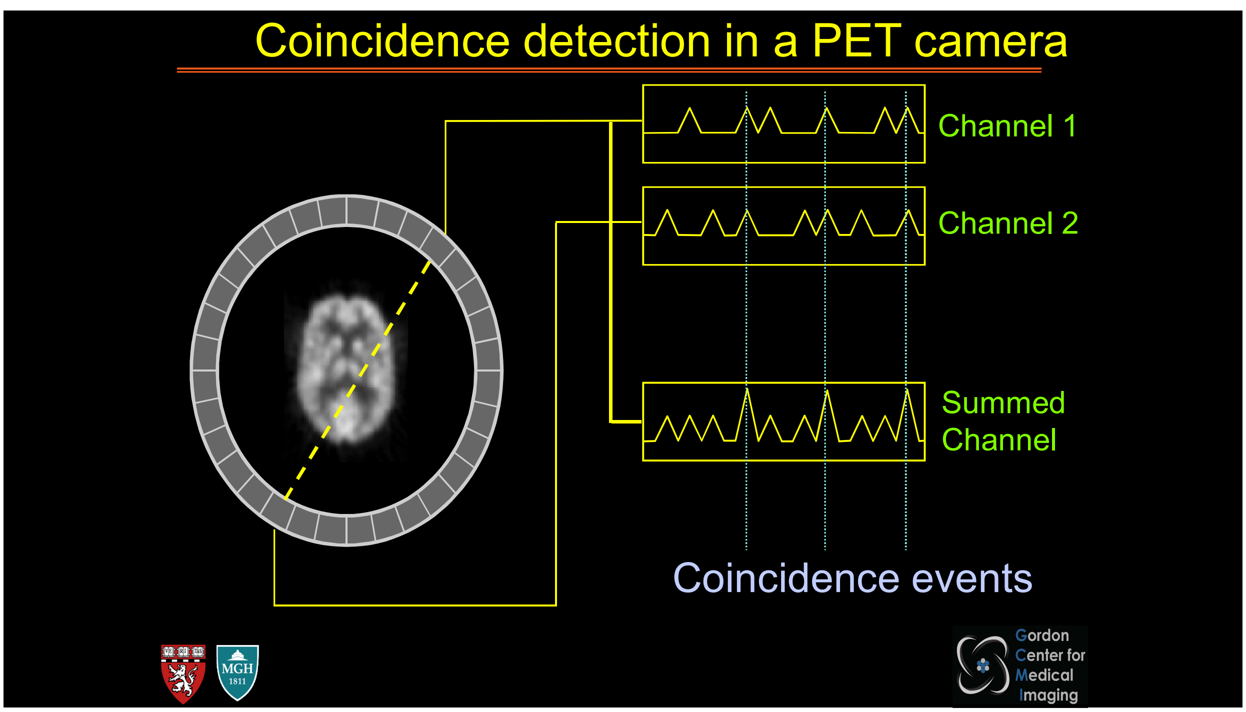
Coincidence detection in a PET camera
Channel 1
Channel 2
Summed Channel
Coincidence events
Gordon Center for Medical Imaging
MGH 1811

A block-detector PET camera consists of detectors in a series of rings

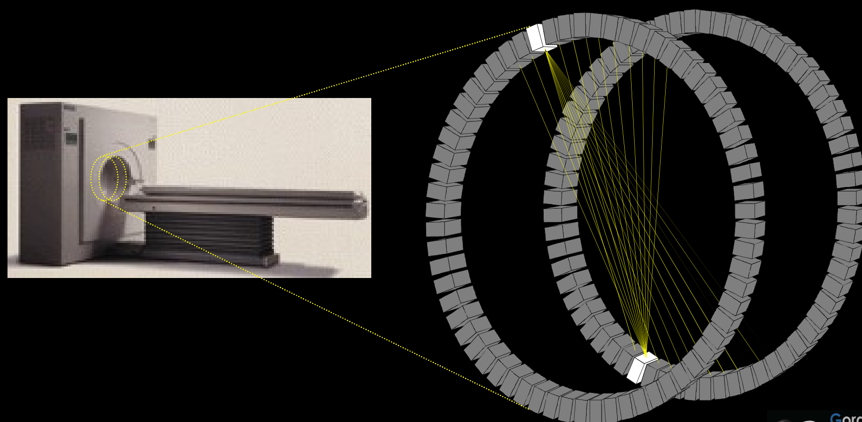

Gordon Center for Medical Imaging

Types of coincidence events

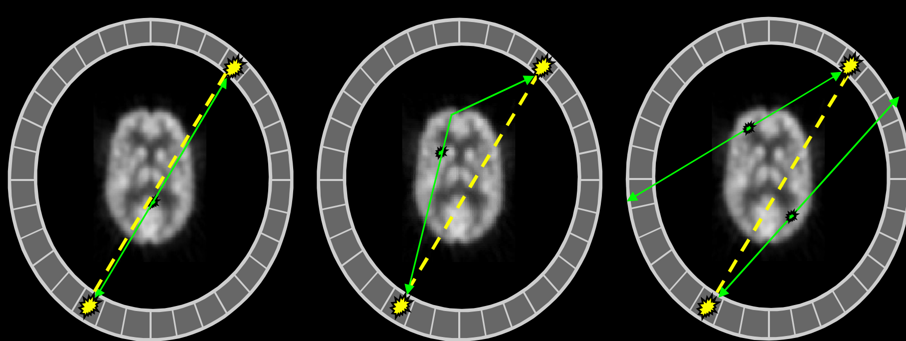

Gordon Center for Medical Imaging

Example: Typical Whole Body PET

Type of coincidence	Percentage (%)
Raw	100
Trues	38
Randoms	34
Scattered	28
Multiple	7

Electronic collimation and intrinsic resolution

- Resolution depends on size of detector elements
- Resolution does not change much between the detectors

Positron range and intrinsic resolution

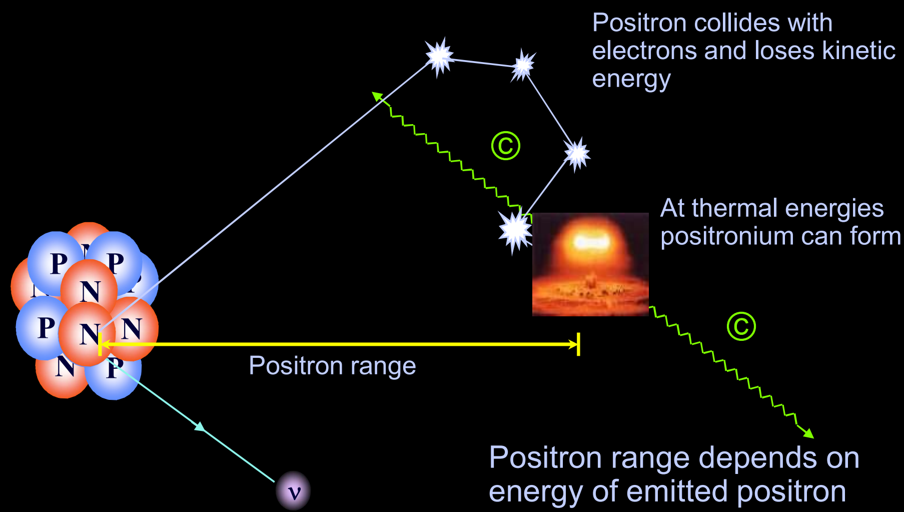

Gordon Center for Medical Imaging

Positron range and intrinsic resolution (2)

Isotope	Maximum positron energy (MeV)	Mean positron energy (MeV)	Range in water FHWM (mm)
^{18}F	0.64	0.25	0.10
^{11}C	0.96	0.39	0.19
^{13}N	1.19	0.49	0.28
^{15}O	1.70	0.74	0.50
^{82}Rb	3.15		1.6

Gordon Center for Medical Imaging

Positron range and intrinsic resolution (3)

Approximate annihilation distribution for ^{18}F and ^{82}Rb in water

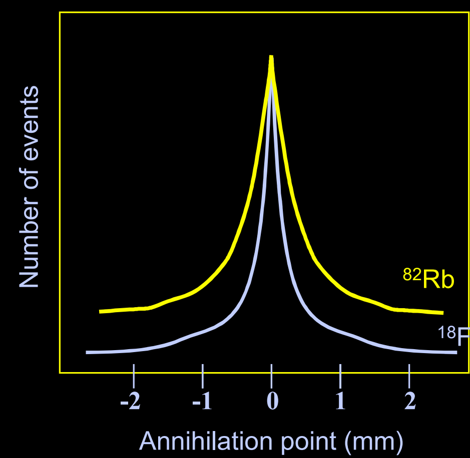

Gordon Center for Medical Imaging

Positron range and intrinsic resolution (4)

^{82}Rb
GE-DST, OSEM

^{13}N-ammonia
Scanditronix, FBP

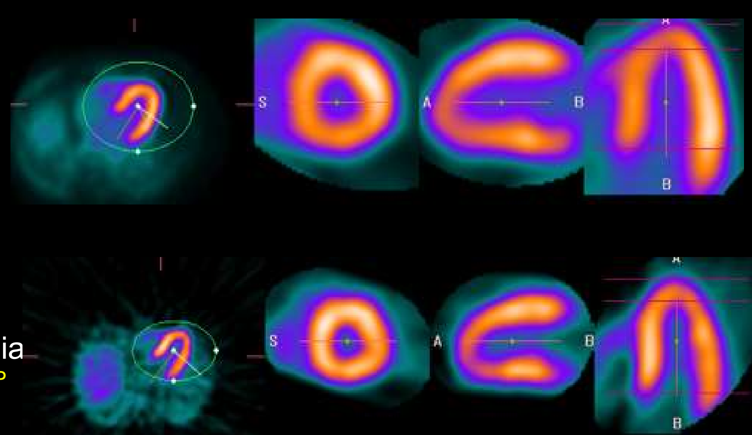

Gordon Center for Medical Imaging

Photon non co-linearity & intrinsic resolution

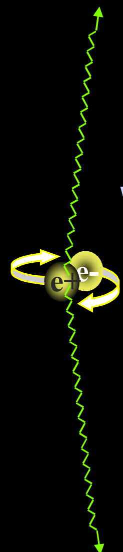

Momentum is conserved.

What happens to the momentum of the positronium?

The annihilation photons must carry it away -
so they are not exactly co-linear.

Angular uncertainty ~ 0.5 degrees

Positional uncertainty for 1m PET scanner ~ 2 mm

Gordon Center for Medical Imaging

Depth of interaction and intrinsic resolution

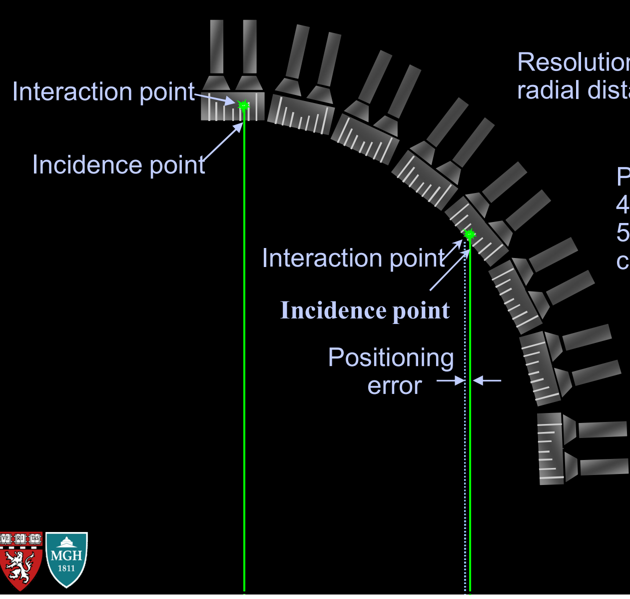

Resolution degrades as the radial distance increases

PET-CT:
4.5 mm at the center
5.5 mm at 10 cm from center

Most clinical tomographs have spatial resolution in 4-6 mm range

Gordon Center for Medical Imaging

General concepts of tomography acquisition

Planar acquisition

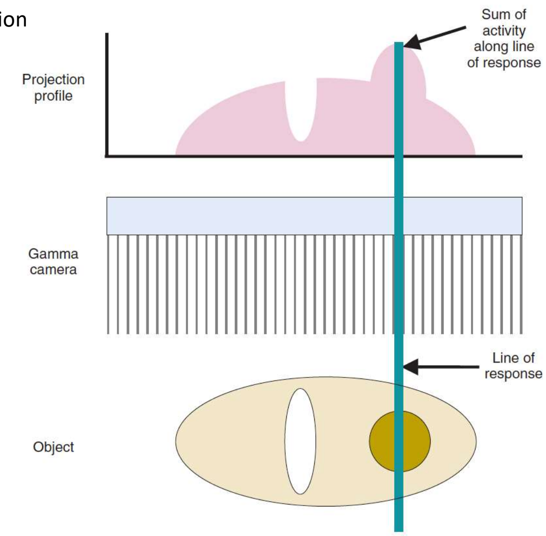

Cherry, S. R.; Sorenson, J. A.; Phelps, M. E. Physics in Nuclear Medicine; Elsevier, 2012.

Gordon Center for Medical Imaging

Projection imaging

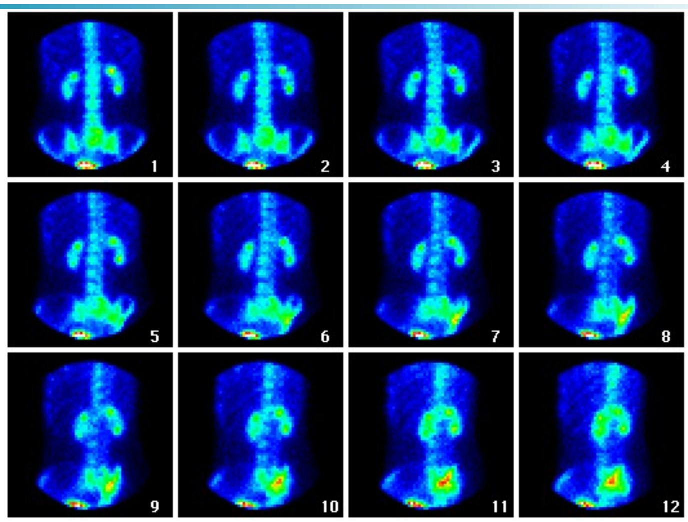

Gordon Center for Medical Imaging

Projection imaging

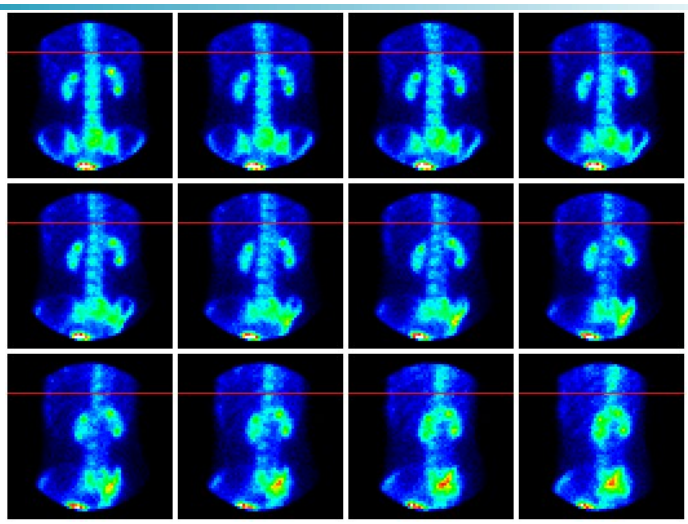

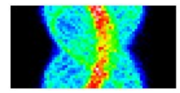

sinogram

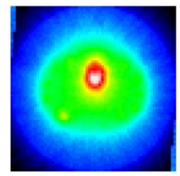

backprojection non filtered

Gordon Center for Medical Imaging

General concepts of tomography acquisition

Tomography: Many planar acquisitions

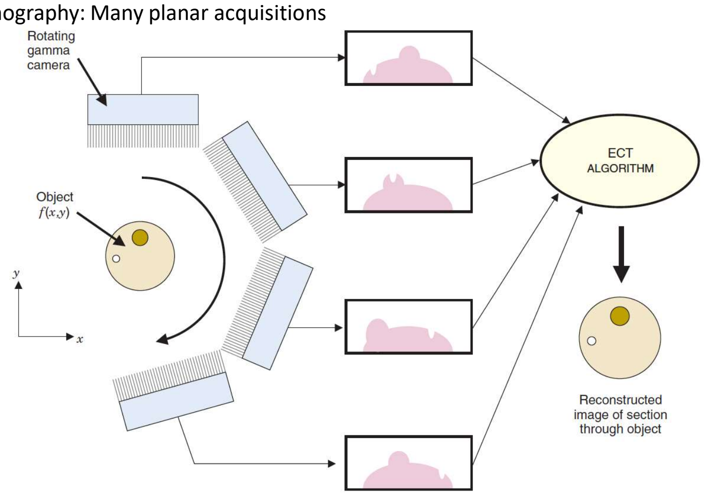

Cherry, S. R.; Sorenson, J. A.; Phelps, M. E. Physics in Nuclear Medicine; Elsevier, 2012.

Gordon Center for Medical Imaging

SPECT scanners

Gordon Center for Medical Imaging

PET scanners

Biograph (Siemens)

Gemini (Philips)

Discovery (GE)

Gordon Center for Medical Imaging

CT scanners

Displaying projection data: Sinogram

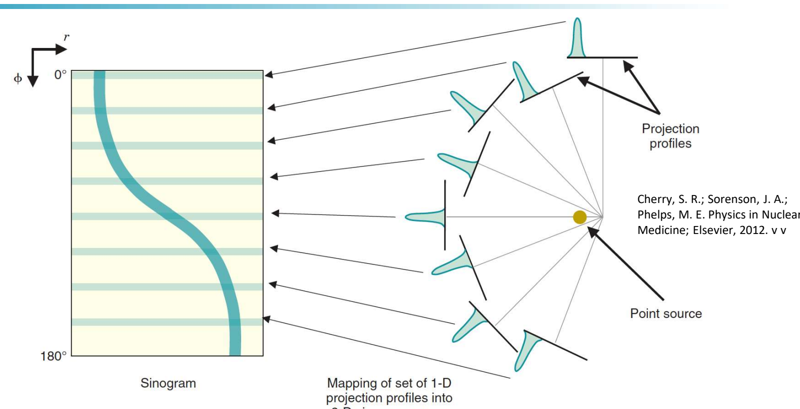

A sinogram is a representation of the projection data in a 2D matrix. Each slice will have its own 2D sinogram.

Tomography: sinogram

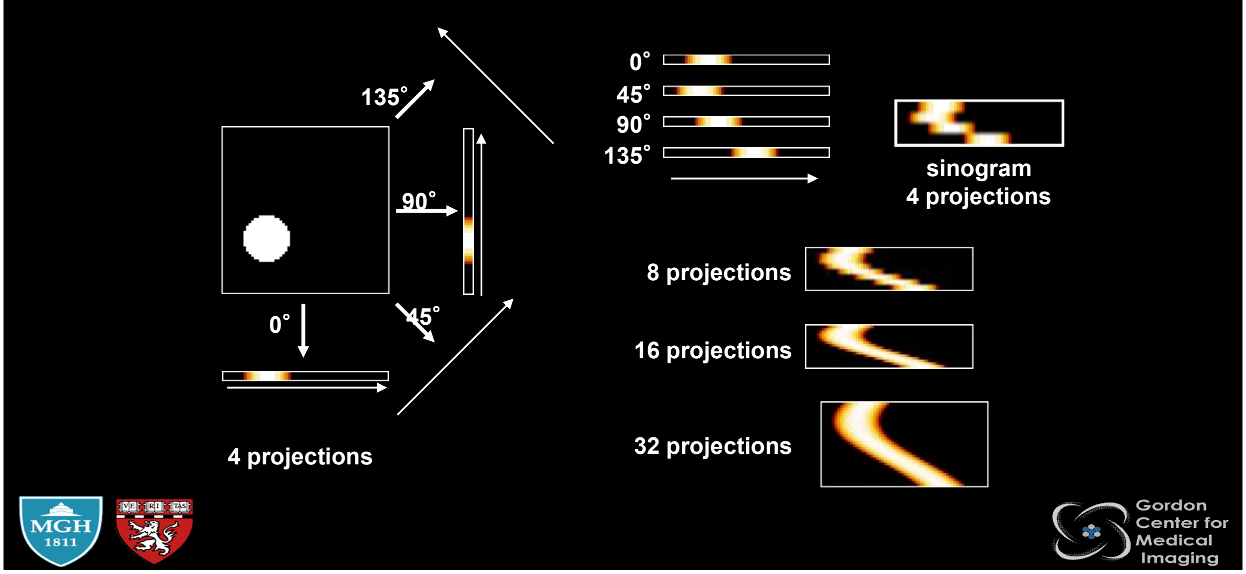

Sinograms are useful for detecting patient motion

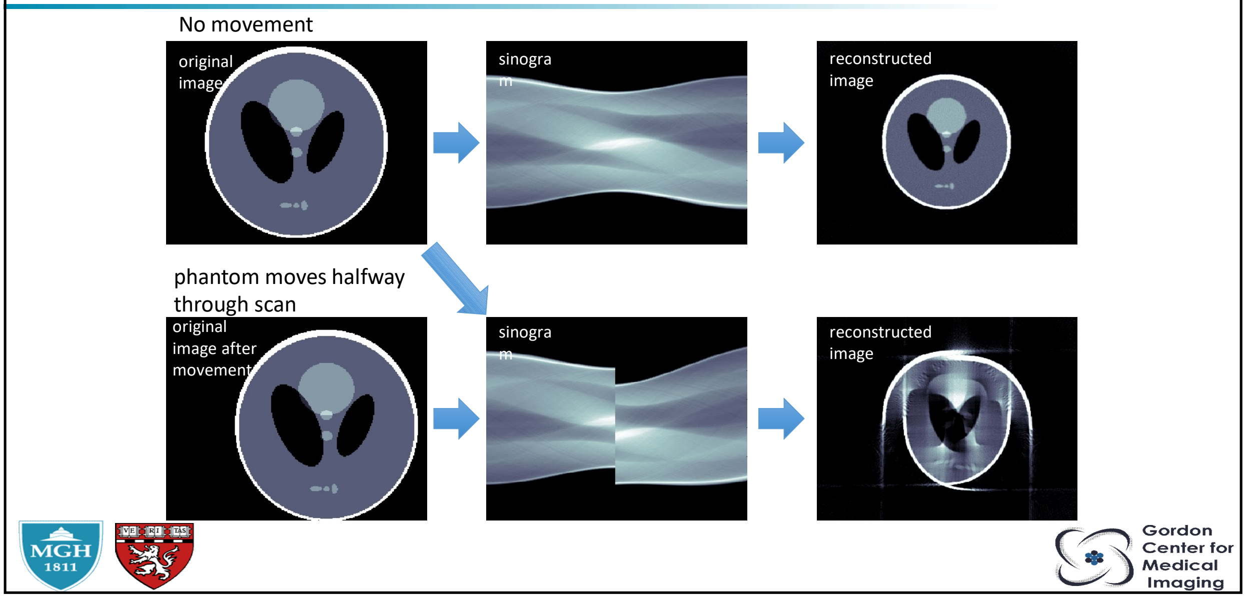

Scanner coordinate system

- Object space (x,y) to scanner space (r,s):

$$r = x\cos\theta + y\sin\theta$$

$$s = y\cos\theta - x\sin\theta$$

- Explains how radioactivity at location (x,y) contributes to signal recorded at location r acquired at rotation angle θ

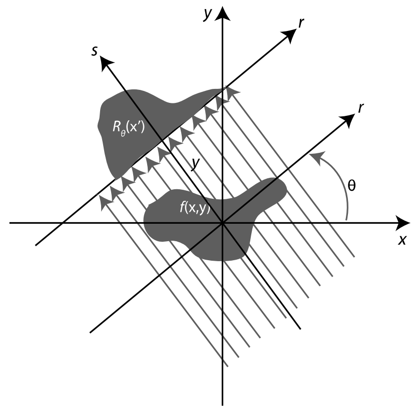

Foundation of backprojection: Radon transform

- An integral transform that takes f(x,y) and defines it as line integrals through f(x,y) at different offsets from the origin

Radon transform:

$$R(r,\theta) = \int_{-\infty}^{\infty}\int_{-\infty}^{\infty} f(x,y)\,\delta\left(\boxed{x\cos\theta + y\sin\theta - r}\right)dxdy$$

Backprojection:

$$b(x,y) = \int_{0}^{\pi} R(r,\theta)\big|_{r=x\cos\theta+y\sin\theta}\,d\theta$$

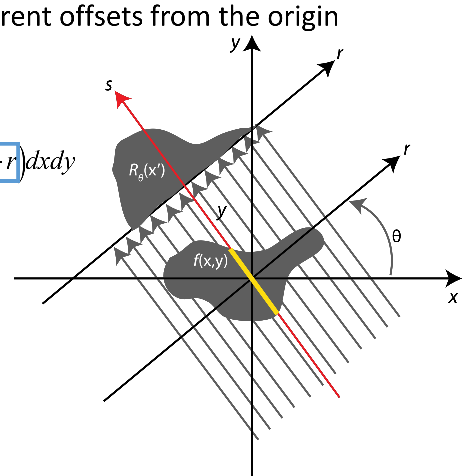

Simple backprojection

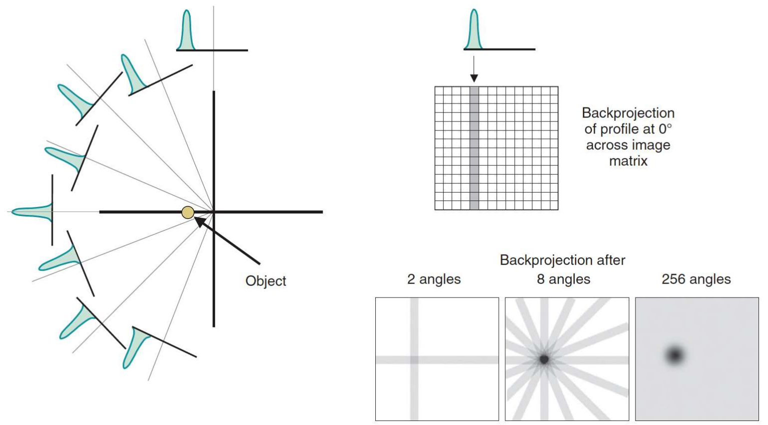

Cherry, S. R.; Sorenson, J. A.; Phelps, M. E. Physics in Nuclear Medicine; Elsevier, 2012.

Gordon Center for Medical Imaging

How does simple backprojection work?

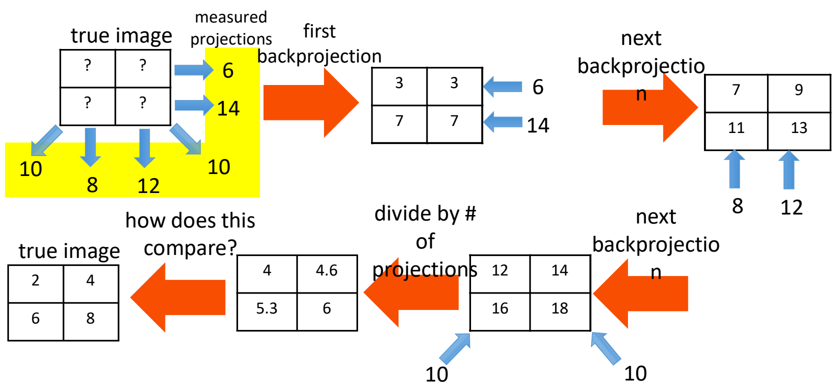

Gordon Center for Medical Imaging

Simple backprojection with no filtering

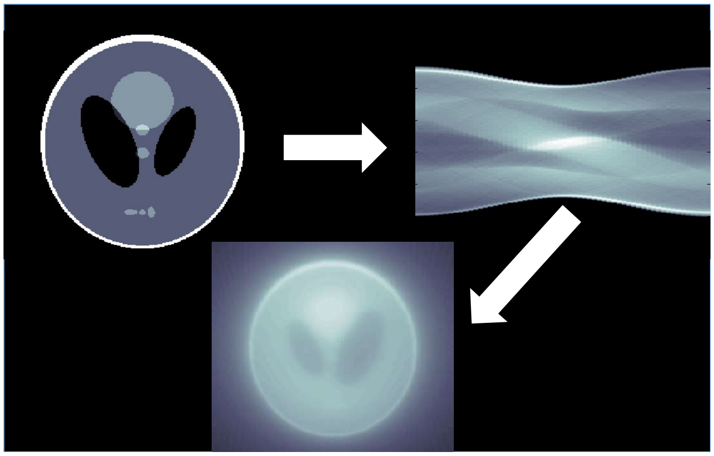

Simple backprojection results in blurring that is mathematically explained as:

$f'(x,y) = f(x,y) * (1/r)$ Often referred to as 1/r blurring.

Gordon Center for Medical Imaging

Central slice theorem

- To solve the 1/r blurring problem of simple backprojection we can use the central slice theorem
- The Fourier transform of a projection of an object at angle, θ, equals a spoke through the 2D Fourier transform of the object that passes through the origin (fx = fy = 0) and is oriented at θ.
- Simple backprojection oversamples in Fourier space

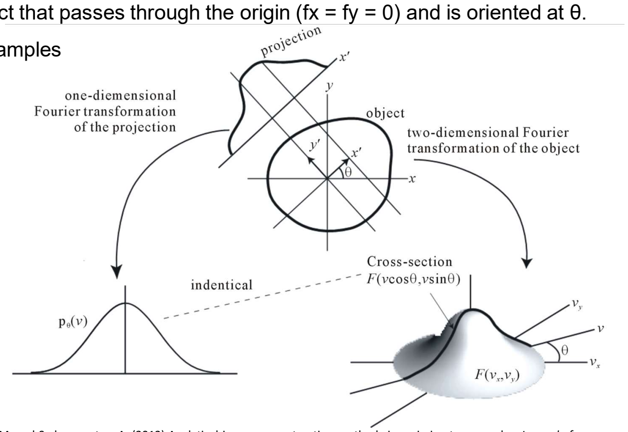

Asl, M. and Sadremomtaz, A. (2013) Analytical image reconstruction methods in emission tomography. *Journal of Biomedical Science and Engineering*, **6**, 100-107. doi: 10.4236/jbise.2013.61013.

Gordon Center for Medical Imaging

Steps for filtered backprojection (FBP)

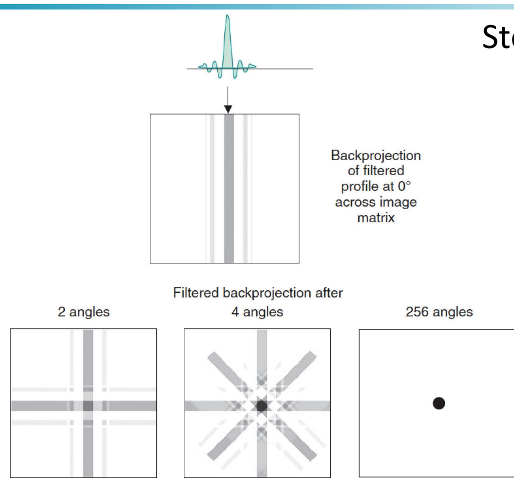

Cherry, S. R.; Sorenson, J. A.; Phelps, M. E. Physics in Nuclear Medicine; Elsevier, 2012.

Steps for FBP

1. Acquire projection images
2. Compute the 1D Fourier transform of each profile (convert to spatial frequency domain)
3. Apply the filter in the frequency domain
4. Compute the inverse Fourier transform to convert back to spatial domain
5. Perform backprojection

Filtered Backprojection: Filters

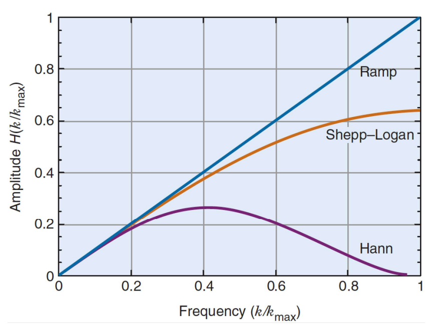

Cherry, S. R.; Sorenson, J. A.; Phelps, M. E. Physics in Nuclear Medicine; Elsevier, 2012.

- Filtering is used to remove the 1/r blurring found in simple backprojection
  - Ramp is simplest
- Others are used to remove noise artifacts at high frequencies
  - Shepp-Logan
  - Hann
- Filtering is performed in spatial frequency space following a Fourier transform

Tomography: filtering

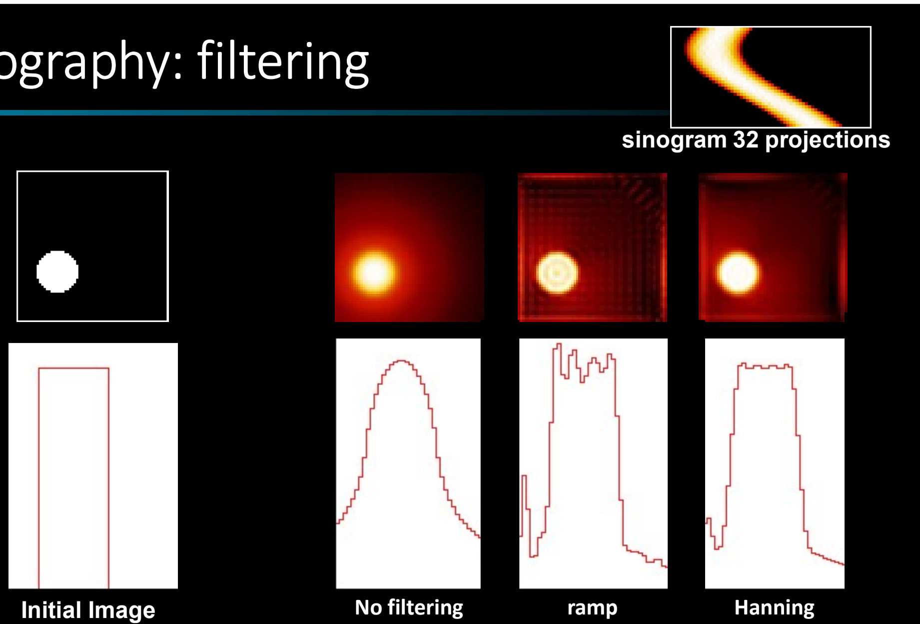

Filtered Backprojection: Equation form

Steps for FBP

1. **Acquire projection images** $p(r,\theta)$
2. **Compute the 1D Fourier transform of each profile (convert to frequency domain)**
3. **Apply the filter in the frequency domain**
4. Compute the inverse Fourier transform to convert back to spatial domain
5. **Perform backprojection**
6. **Then apply this procedure and sum over all projections**

$$f(x,y)=\int_0^\pi d\theta \left[\int_0^\infty d\omega\, |\omega|\, P(\omega)\, e^{2\pi i\omega r}\right]_{r=x\cos\theta+y\sin\theta}$$

Tomography : reconstruction of 1 slice

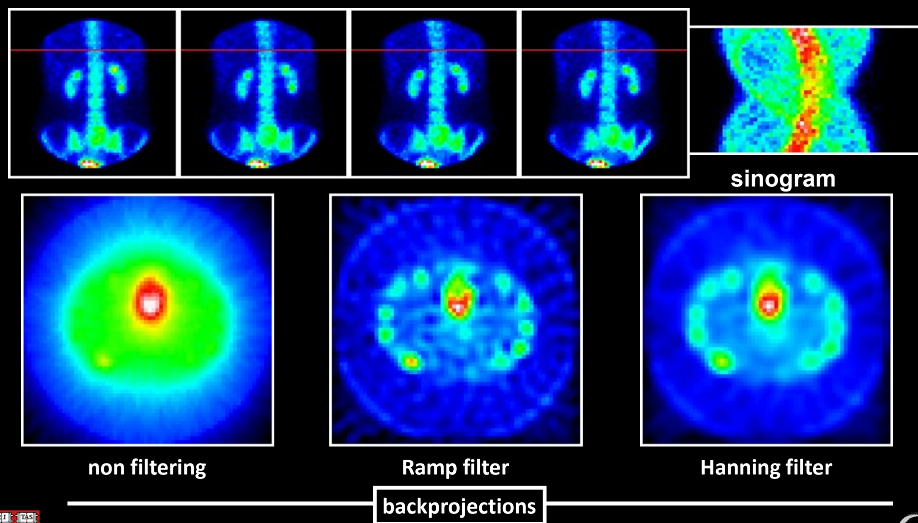

Gordon Center for Medical Imaging

Factors affecting image quality: Noise

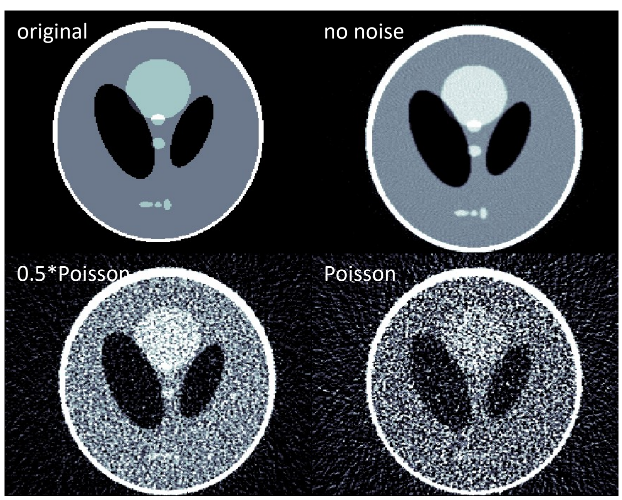

Gordon Center for Medical Imaging

Factors affecting image quality: Acquisition sampling

Low projection sampling resolution can cause blurring and aliasing artifacts

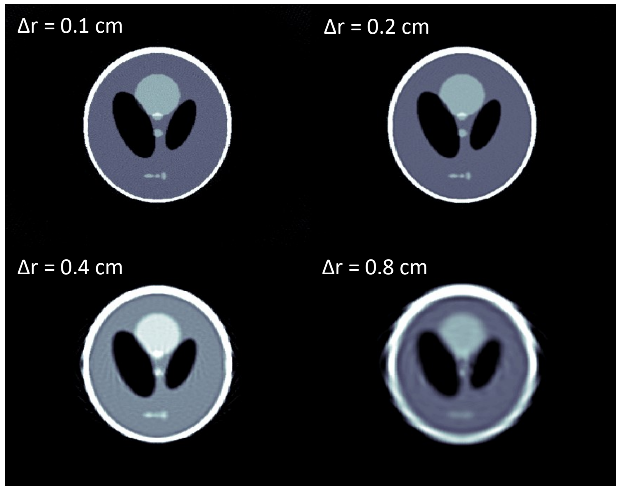

Factors affecting image quality: Reconstruction filter

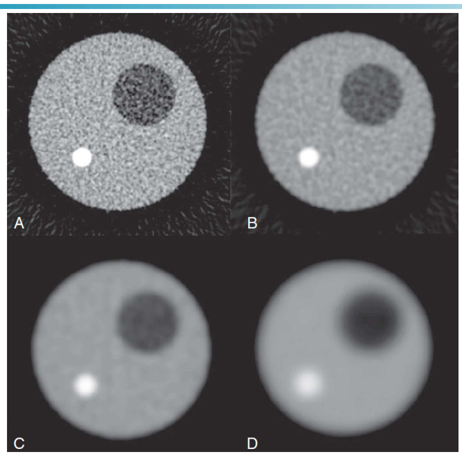

Cherry, S. R.; Sorenson, J. A.; Phelps, M. E. Physics in Nuclear Medicine; Elsevier, 2012.

- Reduction of cutoff frequency:
  - Increase blurring
  - Reduction in noise
  - Reduction in image detail

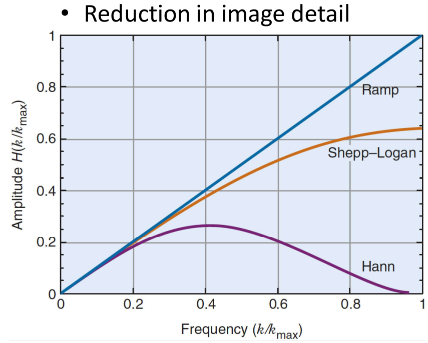

Cherry, S. R.; Sorenson, J. A.; Phelps, M. E. Physics in Nuclear Medicine; Elsevier, 2012.

Factors affecting image quality: Angular sampling

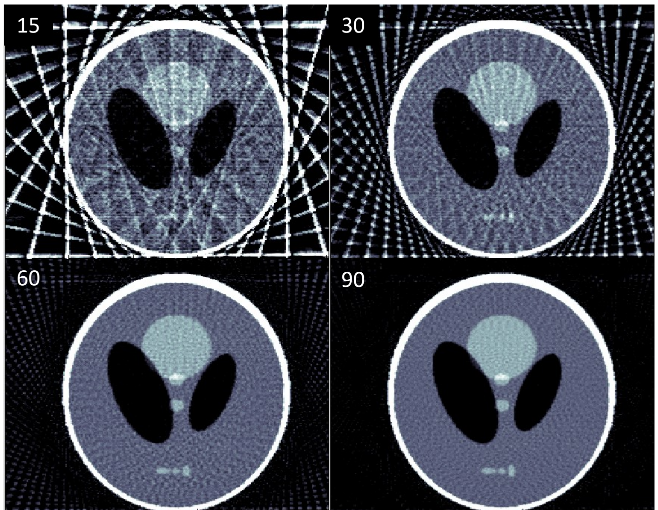

- Reduction in acquired projection angles:
- Decrease acquisition time
- Increase spoke-like artifacts

Factors affecting image quality: Angular sampling range

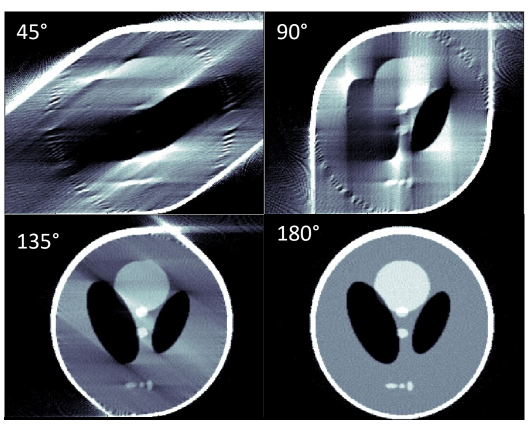

- Full 180° angular sampling is needed

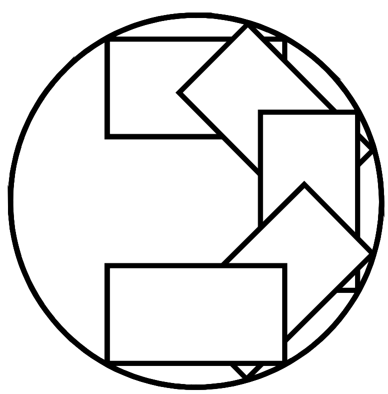

Factors affecting image quality: Full object coverage

- Incomplete coverage of the object during some or parts of the scan can lead to artifacts

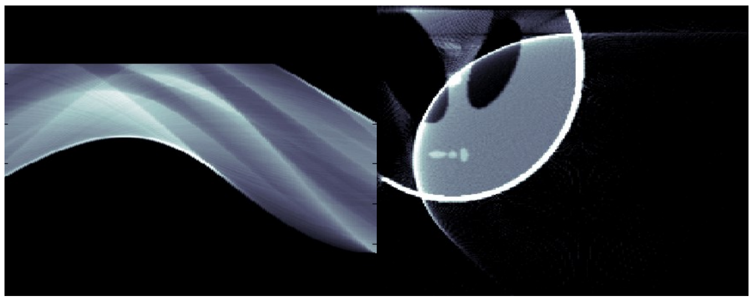

Factors affecting image quality: Missing detector

- Instrumentation failure can cause artifacts due to missing data

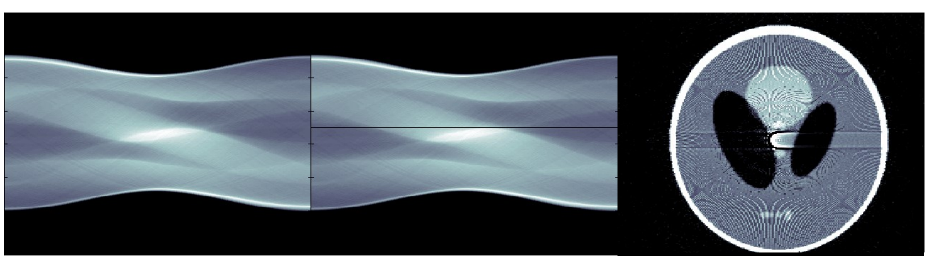

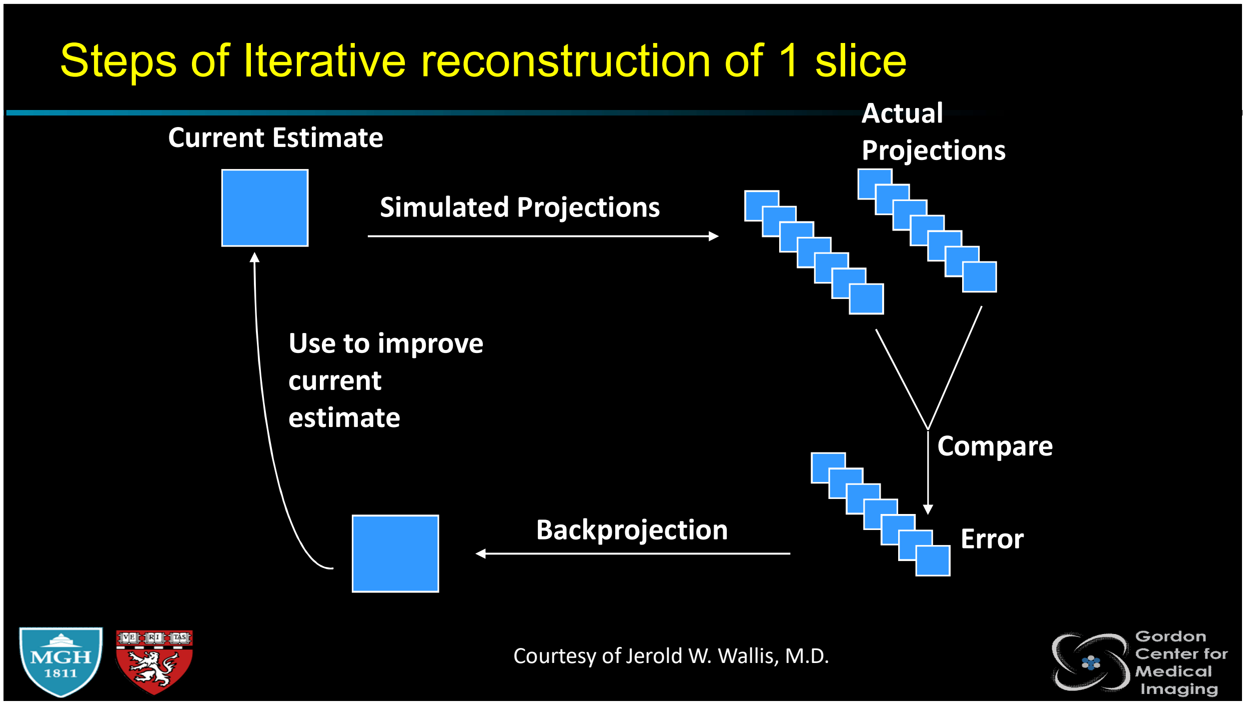
Steps of Iterative reconstruction of 1 slice
Current Estimate
Actual Projections
Simulated Projections
Use to improve current estimate
Compare
Backprojection
Error
Courtesy of Jerold W. Wallis, M.D.
Gordon Center for Medical Imaging

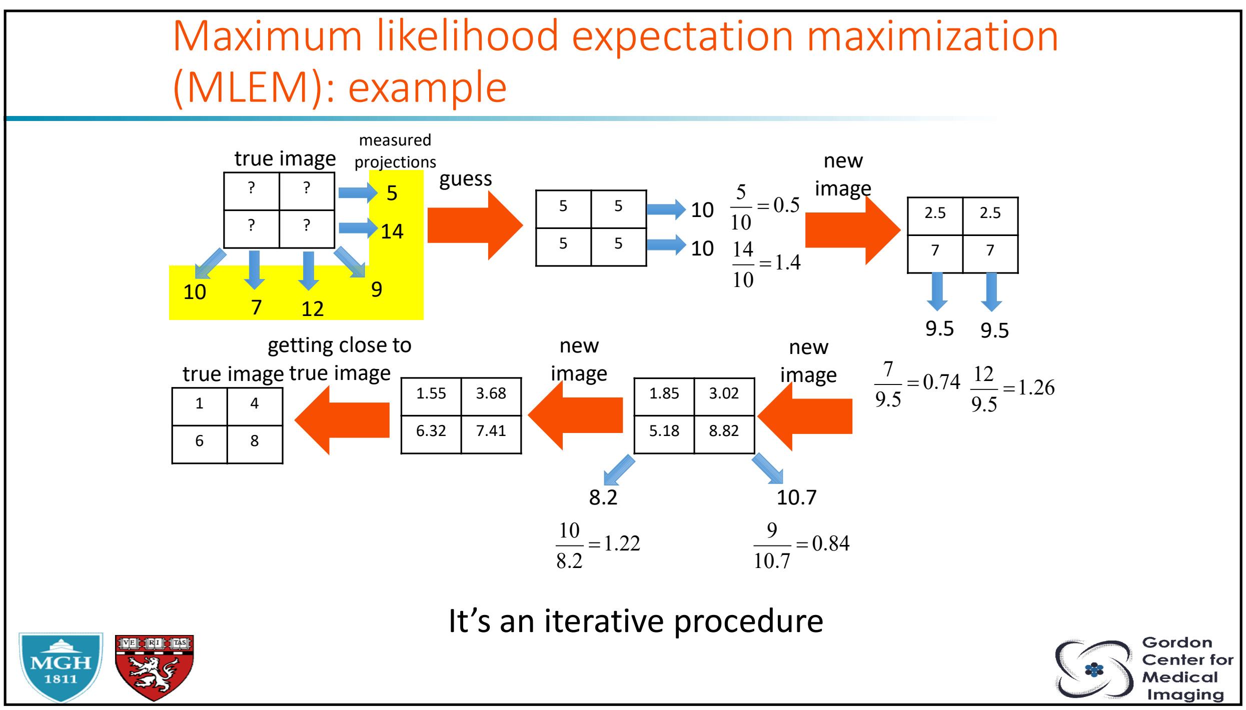
Maximum likelihood expectation maximization (MLEM): example
true image
measured projections
guess
new image
getting close to true image
true image
5
14
10
7
12
9
10
10
$\frac{5}{10} = 0.5$
$\frac{14}{10} = 1.4$
9.5
9.5
$\frac{7}{9.5} = 0.74$
$\frac{12}{9.5} = 1.26$
8.2
10.7
$\frac{10}{8.2} = 1.22$
$\frac{9}{10.7} = 0.84$
It's an iterative procedure
Gordon Center for Medical Imaging

Maximum likelihood expectation maximization (MLEM): Equation form

$$f_i^{(n+1)} = f_i^{(n)} \cdot \frac{1}{\sum_j a_{ij}} \sum_j \frac{g_j}{\sum_k a_{kj} f_k^{(n)}} a_{ij}$$

The current image estimation: $f_i^{(n)}$

The probability that activity emitted in voxel i is detected by detector j: a_{ij}

a_{ij} can contain physical information such as effects of spatial resolution, scatter, attenuation and other characteristics of the detection process

Actual measured projection: g_j

Current forward projection estimate: $\sum_k a_{kj} f_k^{(n)}$

Therefore, the ratio of the measured projection to the current projection is: $\frac{g_j}{\sum_k a_{kj} f_k^{(n)}}$

Current backprojection of this ratio is: $\sum_j \frac{g_j}{\sum_k a_{kj} f_k^{(n)}} a_{ij}$

Which then acts upon the current estimate $f_i^{(n)}$ to form our new estimate $f_i^{(n+1)}$

MGH 1811 VE RI TAS

Gordon Center for Medical Imaging

Steps of maximum likelihood expectation maximization (MLEM): equation form

$$f_i^{(n+1)} = f_i^{(n)} \cdot \frac{1}{\sum_j a_{ij}} \sum_j \frac{g_j}{\sum_k a_{kj} f_k^{(n)}} a_{ij}$$

1. The first $f_i^{(0)}$ is a guess and is typically uniform.

2. Forward project: Simulate the projection measurement from the previous estimate $\sum_k a_{kj} f_k^{(n)}$

3. Compare the forward projected estimate to the actual measured projection $\frac{g_j}{\sum_k a_{kj} f_k^{(n)}}$

4. Next, update (improve) our estimated image using the current information $f_i^{(n+1)} = f_i^{(n)} \cdot \frac{1}{\sum_j a_{ij}} \sum_j \frac{g_j}{\sum_k a_{kj} f_k^{(n)}} a_{ij}$

5. Repeat this until convergence is reached!

MGH 1811 VE RI TAS

Gordon Center for Medical Imaging

Maximum-likelihood, expectation maximization algorithm (MLEM)

- Correct for Poisson noise

- Positivity guaranteed

- Slow compared to FBP

- Acceleration of the process by the “Ordered Subsets (OSEM) approach”: projections are divided into subsets, which are updated at each iteration

- Noise at high iteration numbers (approximation of a continuous function by a pixelated one)

- Noise can be reduced greatly by convolving the noisy image estimate with a gaussian kernel (regularization)

- How to define when to stop?

Gordon Center for Medical Imaging

How do we know when to stop?

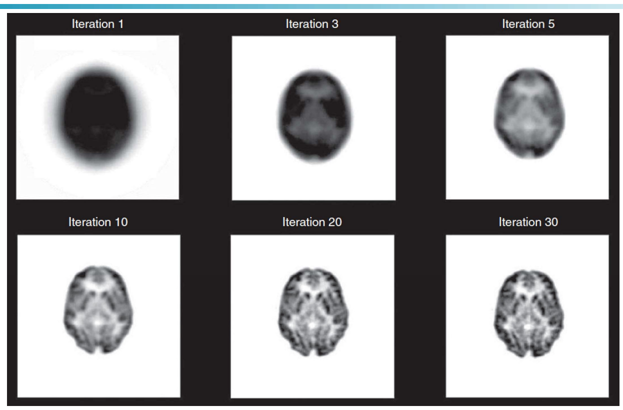

Cherry, S. R.; Sorenson, J. A.; Phelps, M. E. Physics in Nuclear Medicine; Elsevier, 2012.

- Low frequencies are reconstructed first
- As iterations increase image detail is recovered and so is noise
- Too few iterations: no image detail and lack of convergence
- Too many iterations: image is noisy
- Solution: assure proper convergence and remove noise with a gaussian filter

Gordon Center for Medical Imaging

Ordered subset expectation maximization

- Solution to improve MLEM: Ordered-subset expectation maximization (OSEM)
- At each step, project and backproject at only some angles (i.e. a subset)
- Perform the steps in an ordered way to include all angles
- Data start to converge even before the 1st iteration is complete
- Convergence achieved in 3 - 10 iterations
- Much quicker than MLEM

Iterative reconstruction can model the reality of emission tomography

- Attenuation
- Positron range
- Noncollinearity of photons (PET)
- Deadtime
- Scatter coincidences
- Random coincidences
- Physics of crystal: size, intercrystal scatter and penetration
- Noise

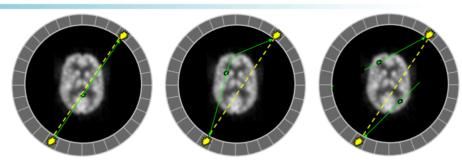

True Coincidence | Scattered Coincidence | Random Coincidence

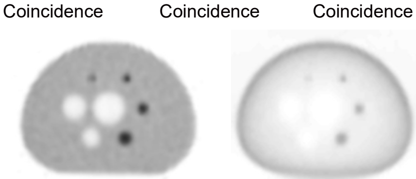

Corrected for attenuation | Not corrected for attenuation

crystal penetration

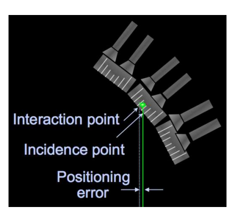

Iterative vs. FBP

- Advantages of iterative methods:
  - The results must be better because the correct physics is included in the reconstruction: The reconstruction algorithm "knows" the physics
  - Attenuation correction
  - Reduction of streak artifact
  - Overall quality
- Disadvantages of iterative methods (MLEM)
  - Slow convergence to the desired solution (e.g. tens - hundreds of iterations)
  - Computationally demanding - number of iterations and inclusion of the physics

Gordon Center for Medical Imaging

OSEM vs FBP

- Filtered Back-Projection
  - Fast
  - Robust
  - Subject to noise & streaks
- OSEM
  - Almost as fast
  - Handles noise & streaks

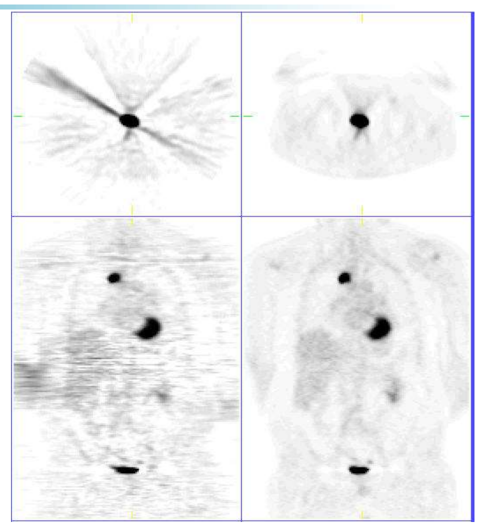

Gordon Center for Medical Imaging

Analytic vs iterative reconstructions

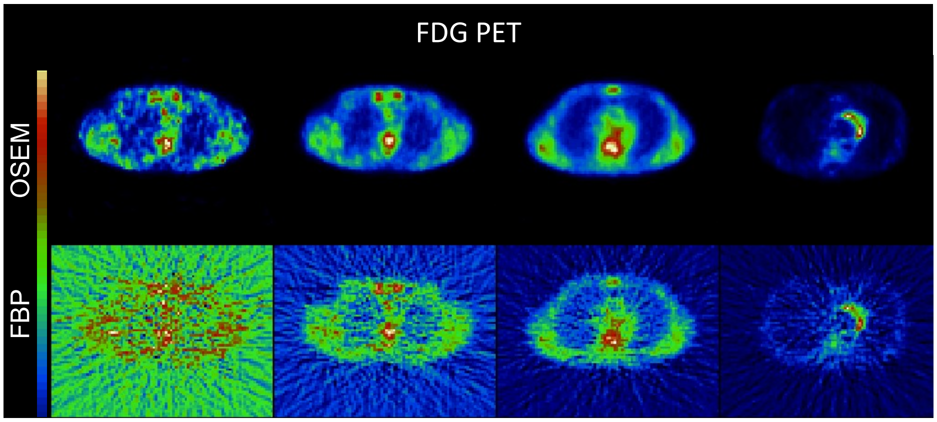

Analytic vs iterative reconstructions

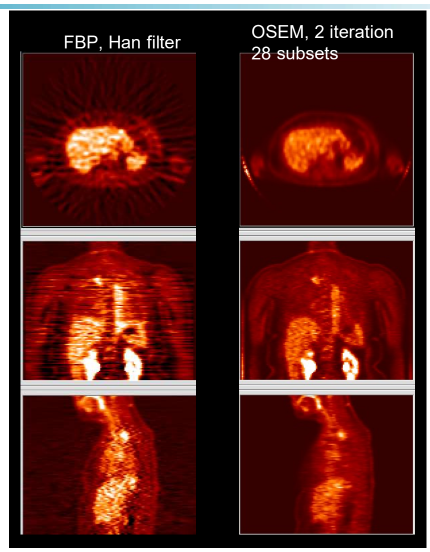

Analytic vs iterative reconstructions

Coronal slices

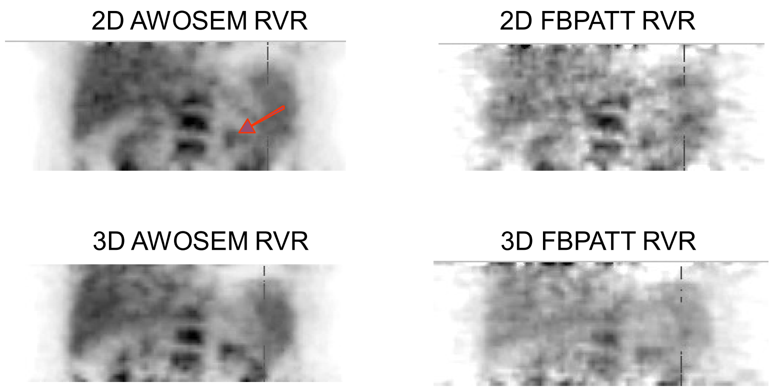

Analytic vs iterative reconstructions

FBP, 10 min emission

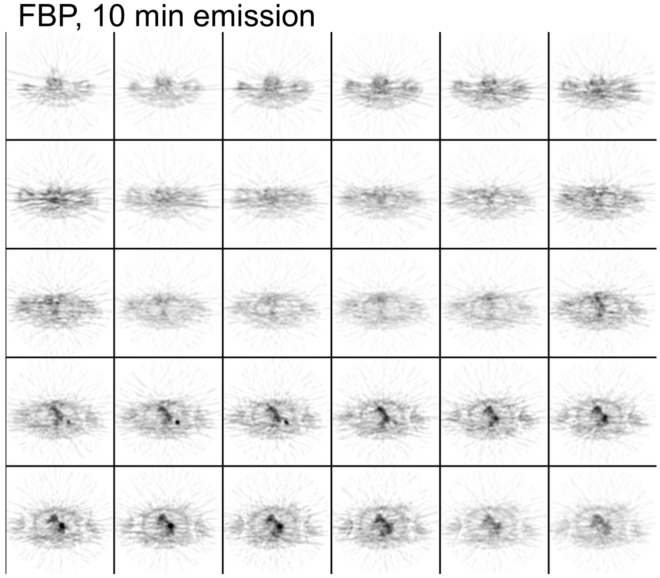

Analytic vs iterative reconstructions

OSEM, 10 min emission

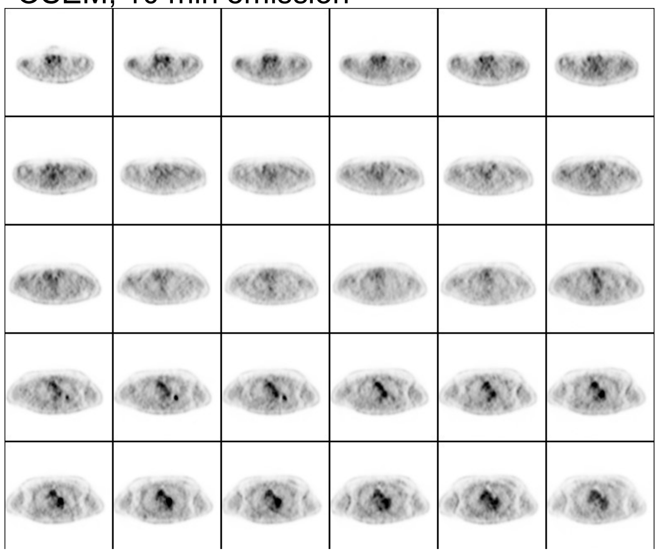

Integrated Whole-Body PET-MR

Simultaneous PET – MR

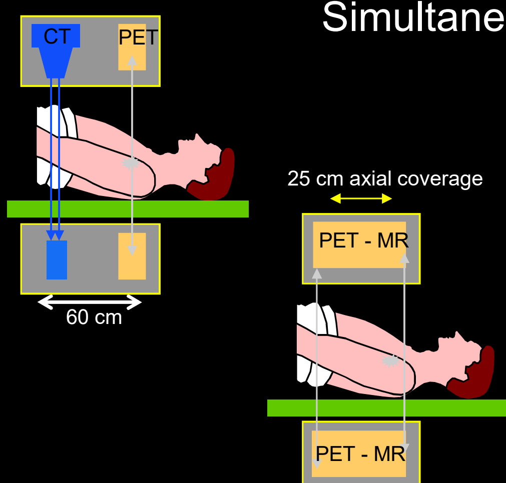

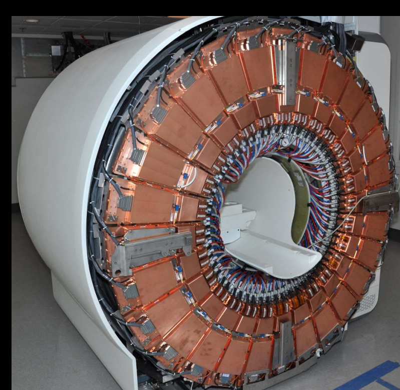

G. El Fakhri, Ph.D.

Methods: Motion Corrected OSEM

- List-mode MLEM reconstruction algorithm with motion modeled in the system matrix:

$$a_{ni}(f)=\sum_{j=1}^{M} a_{nj}\times m_{ji}(f)$$

Motion interpolation matrix (i.e., contribution of pixel i in the ref. frame to pixel j in the deformed frame)

Static system matrix

Number of counts in list-mode

Motion dependent system matrix

$$\rho_i^{(a+1)}=\frac{\rho_i^{(a)}}{\sum_{f=1}^{F} s_i(f)}\sum_{n=1}^{N}\frac{a_{ni}(f_n)}{\sum_{j=1}^{M} a_{nj}(f_n)\,\rho_j^{(a)}}$$

- Attenuation correction using deformed attenuation maps at each frame:

Transformation using measured motion fields from tagged MR

Attenuation map in the reference frame

Attenuation maps in the deformed frames

Gordon Center for Medical Imaging

Ouyang J., Petibon Y., El Fakhri G.

MGH 1811

Primate Results: Acquisition

- Motion Correction with *Primate* in simultaneous PET-MR

Gated tagged MR

Gated PET

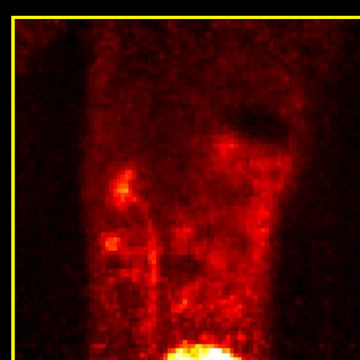

Gordon Center for Medical Imaging

Chun et al. J. Nucl. Med. 2012

MGH 1811

Nonhuman Primate Results (2/3)

JNM
The Journal of Nuclear Medicine

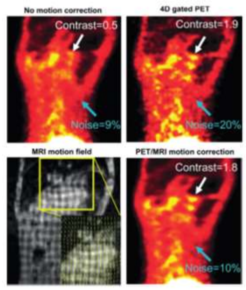

Respiratory and cardiac motion is the most serious limitation to whole-body PET. Here, reconstructed PET images of a freely breathing monkey show that MRI-based motion correction in simultaneous PET/MRI increases contrast and resolution but does not increase noise. This results in significant improvement in PET image quality and is a compelling rationale for further evaluation in clinical studies.

See page 1291.

SNMMI SOCIETY OF NUCLEAR MEDICINE AND MOLECULAR IMAGING

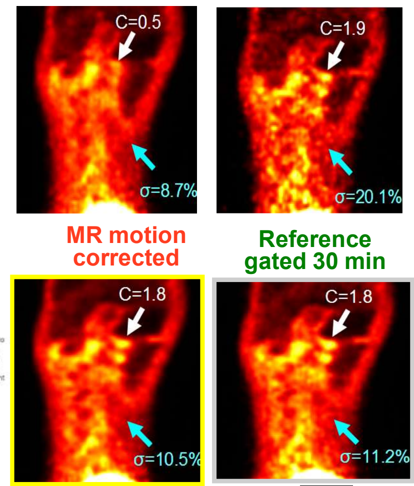

Chun S.Y., Reese T., Guerin B., Catana C., Zhu X., Alpert N., El Fakhri G.
Tagged MR-based Motion Correction in Simultaneous PET-MR. *JNM* 2012;

Liver patient study (1/3)

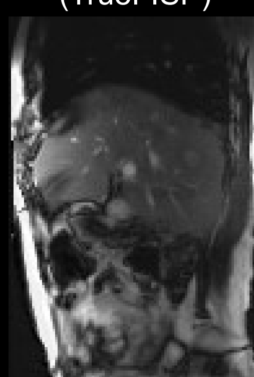

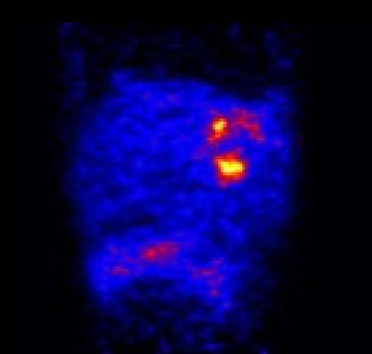

Respiratory motion amplitude in the dome of the liver (~0.7-1.5cm).

Gordon Center for Medical Imaging

Petibon, Huang, Ouyang and El Fakhri.
Relative role of MR-based motion in WB PET-MR. Med. Phys., 2014 41

Initial results in hepatic lesions (2)

- Estimated Motion via B-spline non-rigid image registration

$$\boxed{\hat{T} = \arg\min\left[\Psi_{SSD}\left(I_{tar}, TI_{src}\right)\right] + \eta R(T)}$$

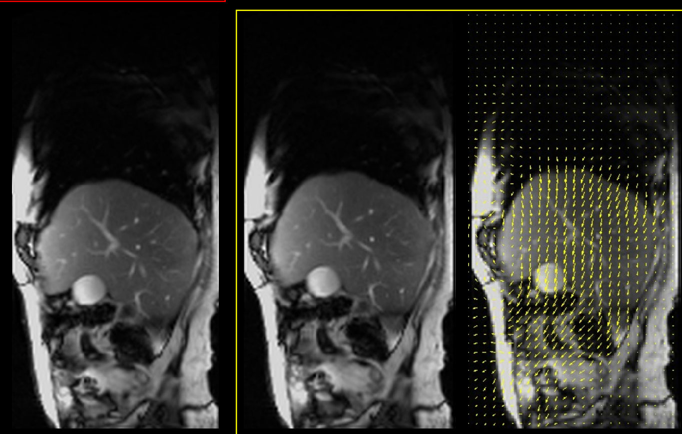

Reference : End-inspiration (I_{src}) End-exhalation (I_{tar})

Gordon Center for Medical Imaging

G. El Fakhri, Ph.D.

Liver patient study (3/3)

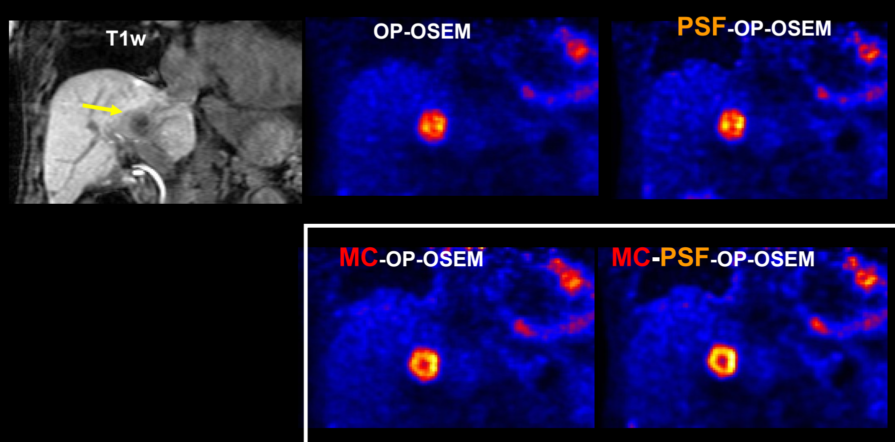

Gordon Center for Medical Imaging

Petibon, Huang, Ouyangand El Fakhri.
Role of MR-based motion and PSF corrections in WB PET-MR. Med. Phys., 2014

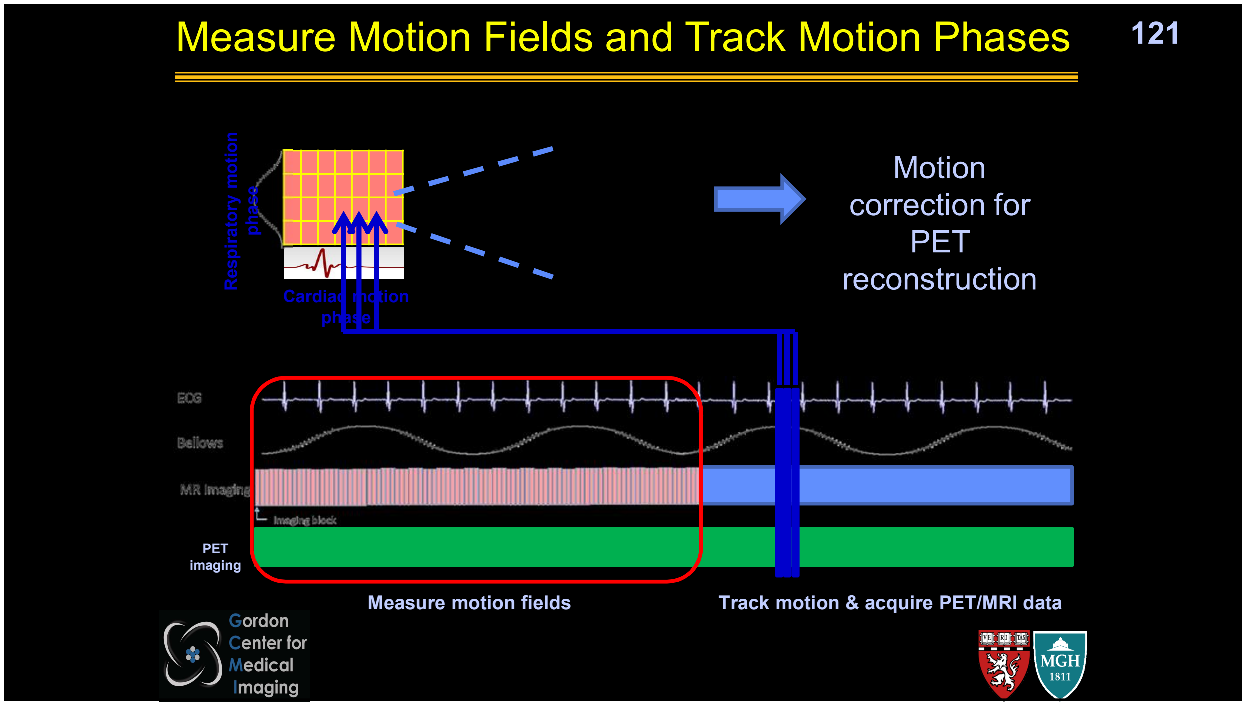

Summary

- PET 101
- Tomography in medical imaging
- Projection imaging
- Sinogram
- Reconstruction-analytic
- Backprojection artifacts
- Reconstruction-iterative
- Comparison of analytic and iterative reconstructions
- Simultaneous PET-MR

MGH 1811

Gordon Center for Medical Imaging

Quantitative Reconstruction in PET / CT and PET / MR

THANK YOU!

MASSACHUSETTS GENERAL HOSPITAL

Gordon Center for Medical Imaging

HARVARD MEDICAL SCHOOL

THE DEPARTMENT OF BIOMEDICAL ENGINEERING

Getting More Image Quality with Less Data in X-Ray CT

J. Webster Stayman

Advanced Imaging Algorithms and Instrumentation Lab (aiai.jhu.edu)
Johns Hopkins University

August 30, 2018

CT Hardware Basics

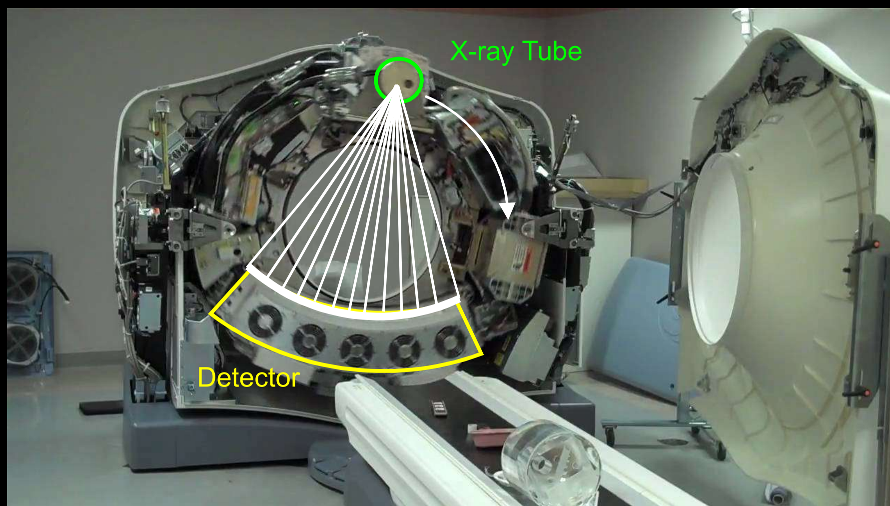

(image Credit) https://www.youtube.com/watch?v=bg0iNhw2ARw

X-ray Tube Physics and Dose Reduction

Number of photons ∝ mA

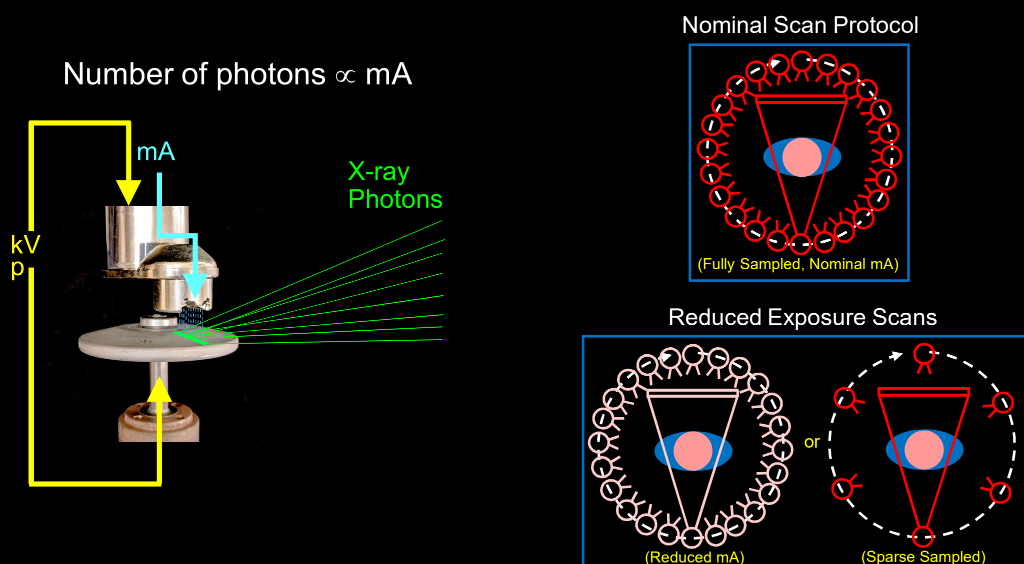

Noise in X-ray Projection Data

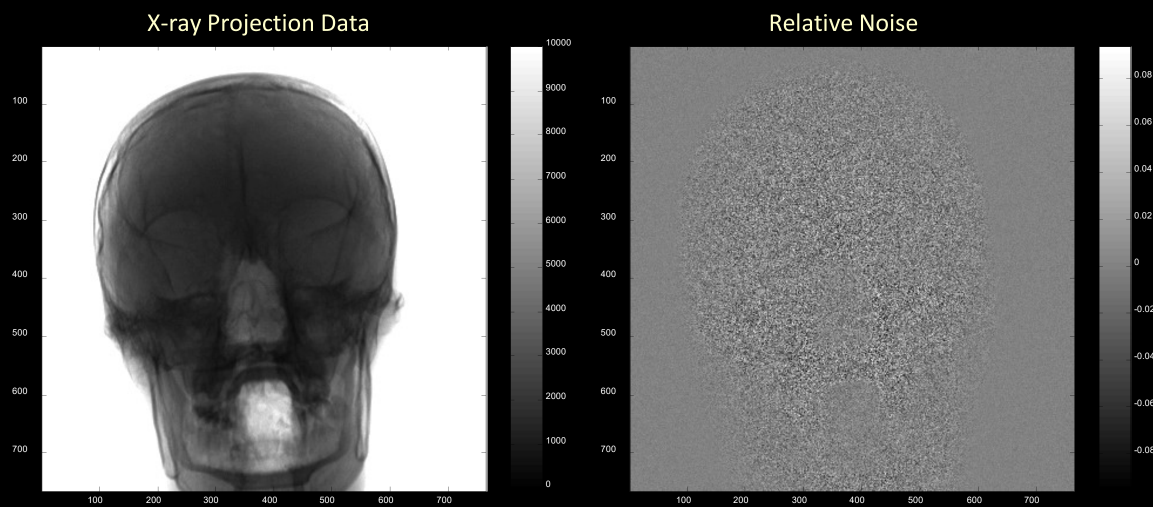

Modeling Projection Data

Discrete-Discrete Parameterization

$$\bar{y}_i = I_0 \exp\left(-\sum_{j=1}^{p} a_{ij}\mu_j\right)$$

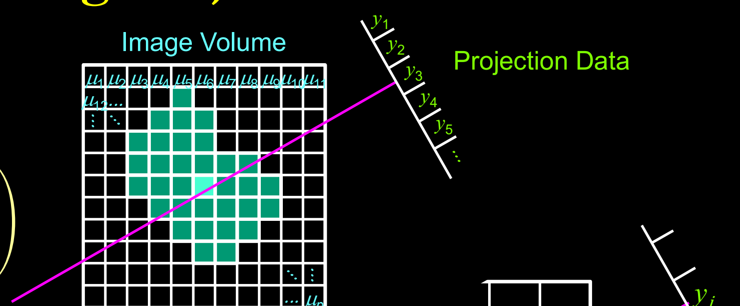

System matrix

$$\mathbf{A} = \begin{bmatrix} a_{11} & \cdots & a_{1j} & \cdots & a_{1p} \\ \vdots & \ddots & \vdots & & \vdots \\ a_{i1} & \cdots & a_{ij} & \cdots & a_{ip} \\ \vdots & & \vdots & \ddots & \vdots \\ a_{n1} & \cdots & a_{nj} & \cdots & a_{np} \end{bmatrix}$$

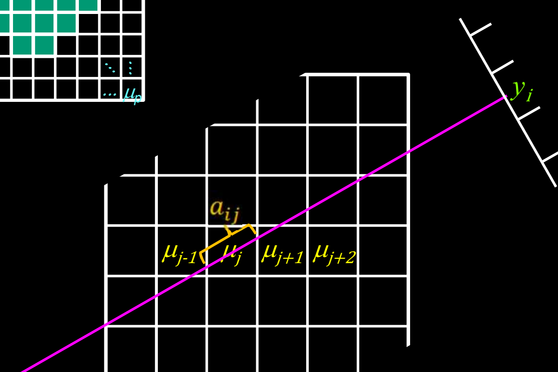

Mathematical Forward Model

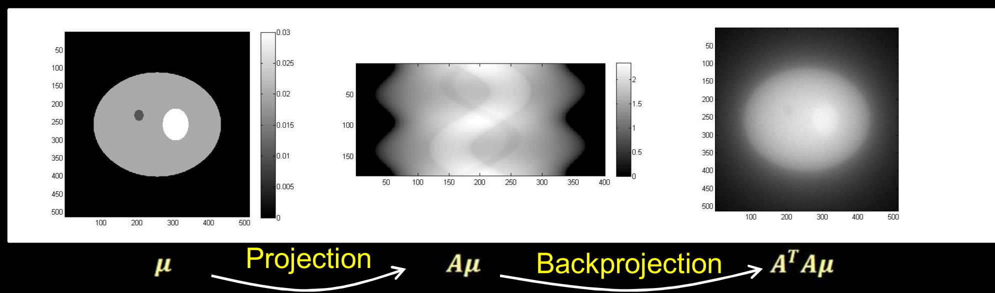

Mean measurements as a function of parameters

$$\bar{y}(\mu) = I_0 \exp(-\mathbf{A}\mu)$$

How to deal with unequal measurement noise (Simple Estimation Problem)

3 Random Variables
Different std dev $(\sigma_1, \sigma_2, \sigma_3)$

Best way to estimate μ?

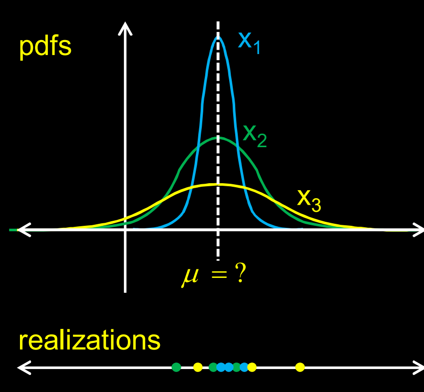

Maximum Likelihood Estimation

Find the parameter values most likely to be responsible for the observed data.

Likelihood Function $L(\boldsymbol{x};\boldsymbol{\mu}) = p(x_1, x_2, \dots, x_N | \mu_1, \mu_2, \dots, \mu_M)$

$$L(\boldsymbol{x};\mu) = p(\boldsymbol{x}|\mu) = \prod_{i=1}^{3} p(x_i|\mu) \qquad p(x_i|\mu) = \frac{1}{\sqrt{2\pi\sigma_i^2}} \exp\left(-\frac{1}{2\sigma_i^2}(x_i-\mu)^2\right)$$

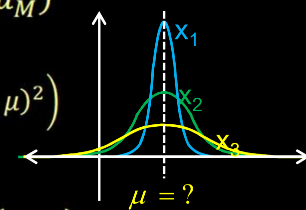

Maximum Likelihood Objective Function $\hat{\boldsymbol{\mu}} = \operatorname{argmax} L(\boldsymbol{x};\boldsymbol{\mu})$

$$\frac{\partial}{\partial\mu}\log L(\boldsymbol{x};\mu) = \sum_{i=1}^{3} \frac{1}{\sigma_i^2}(x_i-\mu) \quad \xRightarrow[\frac{\partial}{\partial\mu}=0]{} \quad \boxed{\hat{\mu} = \frac{\sum_{i=1}^{3} \frac{x_i}{\sigma_i^2}}{\sum_{i=1}^{3} \frac{1}{\sigma_i^2}}}$$

Maximum Likelihood Estimation for CT

Log transformed data case (e.g. $l = -\log\left[\frac{y}{I_0}\right]$)

$$\bar{l}(\mu) = A\mu \qquad P_{l_i} = \frac{1}{\sqrt{2\pi\sigma_i^2}} \exp\left(-\frac{1}{2\sigma_i^2}\left(l_i - \bar{l}_i(\mu)\right)^2\right)$$

Likelihood-based Objective $\log L(y;\mu) = -\cancel{\sum_i^N \frac{1}{2}\log(2\pi\ {}_i^2)} - \sum_i^N \frac{1}{2\sigma_i^2}(l_i - [\mathbf{A}\mu]_i)^2$

$$\cong \boxed{-[l-\mathbf{A}\mu]^T \mathbf{D}\left\{\frac{1}{\sigma_i^2}\right\}[l-\mathbf{A}\mu] = -\|l-\mathbf{A}\mu\|_{\Sigma^{-1}}^2}$$

Solve for μ $\quad \hat{\mu} = \operatorname{argmax} \log L(y;\mu) = \left[\mathbf{A}^T \mathbf{D}\left\{\frac{1}{\sigma_i^2}\right\}\mathbf{A}\right]^{-1} \mathbf{A}^T \mathbf{D}\left\{\frac{1}{\sigma_i^2}\right\} l$

Statistical vs Nonstatistical Reconstruction

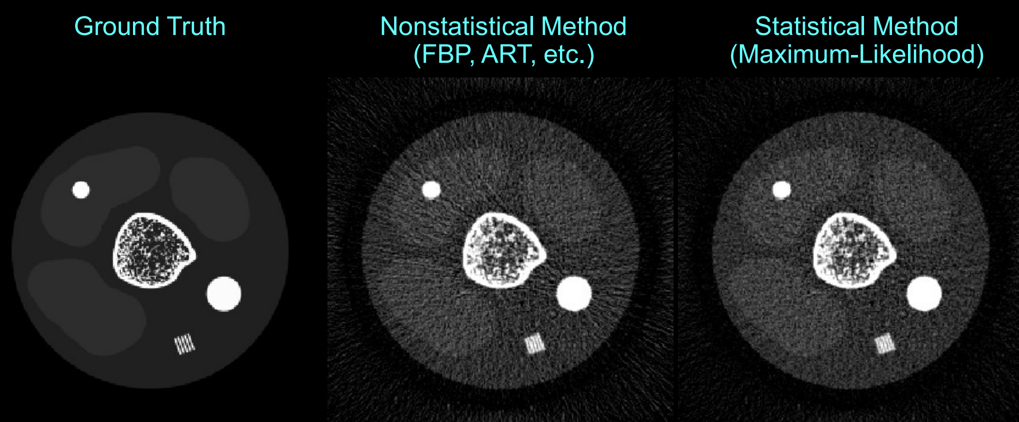

Statistical methods weigh important of individual data points
BUT noise control requires additional information

Additional Information through Regularization

Integrating information via a change in the objective function

$$\hat{\mu} = \operatorname{argmax} \log L(y;\mu) - \beta R(\mu)$$

Penalized-Likelihood Estimation

Choices of regularization $R(\mu)$

- Local smoothness
- Edge-preservation
- Prior images
- Patches/dictionaries/learned regularization

Regularization of Local Image Properties

Pairwise Penalty

$$R(\mu)=\sum_{j}\sum_{k\in N} w_{jk}\psi\left(\mu_j-\mu_k\right)$$

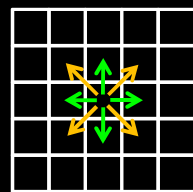

$$k_{1st}=\begin{bmatrix} & -1 & \\ -1 & 4 & -1 \\ & -1 & \end{bmatrix} \quad k_{2nd}=\begin{bmatrix} \frac{-1}{\sqrt{2}} & -1 & \frac{-1}{\sqrt{2}} \\ -1 & 4+\frac{4}{\sqrt{2}} & -1 \\ \frac{-1}{\sqrt{2}} & -1 & \frac{-1}{\sqrt{2}} \end{bmatrix}$$

Penalty Choices

Quadratic $\psi(t)=t^2$

Truncated Quadratic $\psi(t;\delta)=[t^2]_\delta$

Lange $\psi(t;\delta)=\delta\left[\left|\frac{t}{\delta}\right|-\log\left[1+\left|\frac{t}{\delta}\right|\right]\right]$

P-norm $\psi(t;p)=\frac{1}{p}|t|^p$

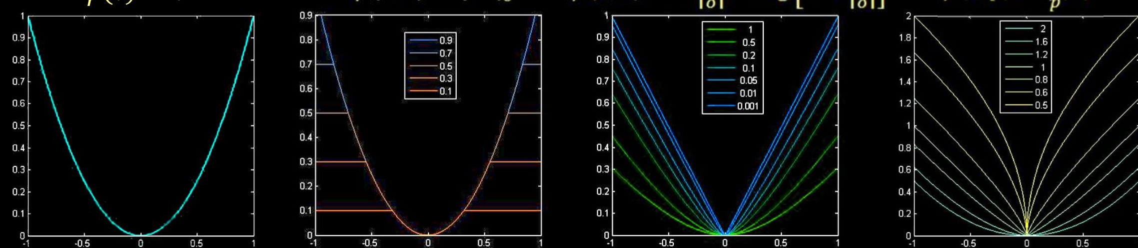

FBP vs (Quadratic) Penalized-Likelihood

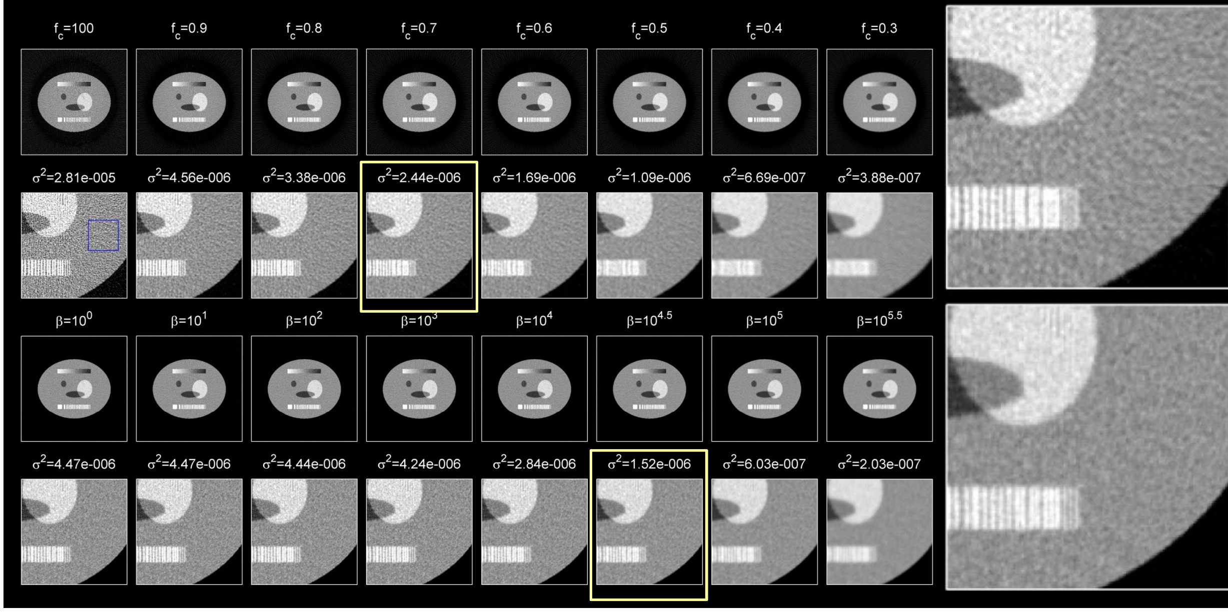

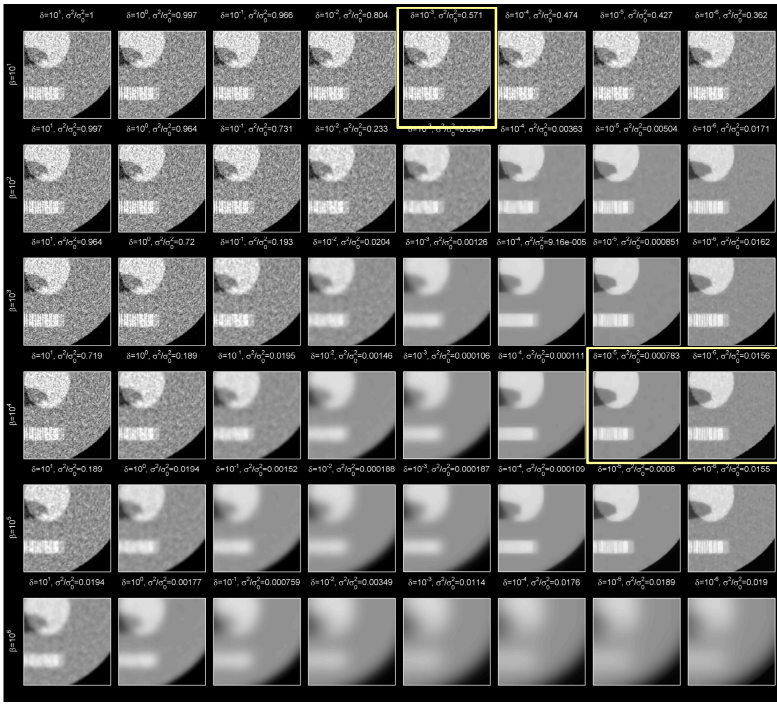

Nonquadratic Penalty (Lange)

$\delta=10^{-3}$, $\sigma^2/\sigma_0^2=0.571$

$\delta=10^{-5}$, $\sigma^2/\sigma_0^2=0.000783$ $\delta=10^{-6}$, $\sigma^2/\sigma_0^2=0.0156$

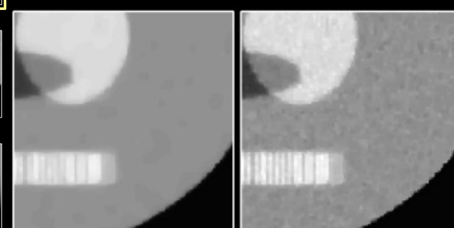

Regularization using Prior Images

Knowledge of anatomy
- Target locations
- Previous imaging studies
  - Post-treatment assessments
  - Monitoring disease progression
  - Dynamic studies

Initial Scan Follow-up Scan (+6 months)

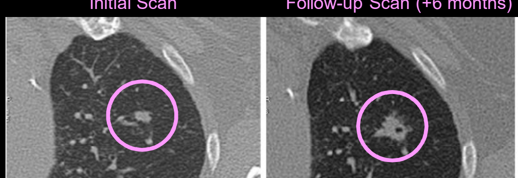

**Image credit: Y. T. and F. W. Poon, "Imaging of solitary pulmonary nodule—
a clinical review," Quant. Im. in Med. and Surg. 3(6), Dec. 2013

Prior Image Registration Penalized-Likelihood Estimation (PIRPLE)

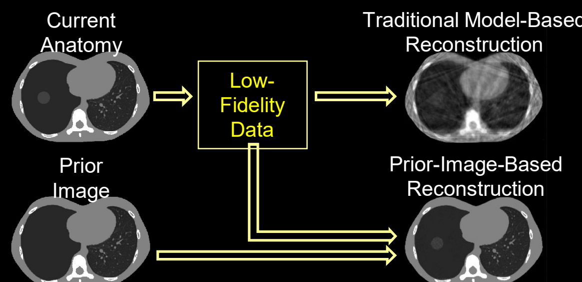

$$\{\hat{\mu}, \hat{\lambda}\} = \operatorname{argmax} \log L(y;\mu) - \beta_R R(\mu) - \beta_P \|\mu - \mathbf{W}(\lambda)\mu_P\|_1$$

Prior Image Registration Penalty Term

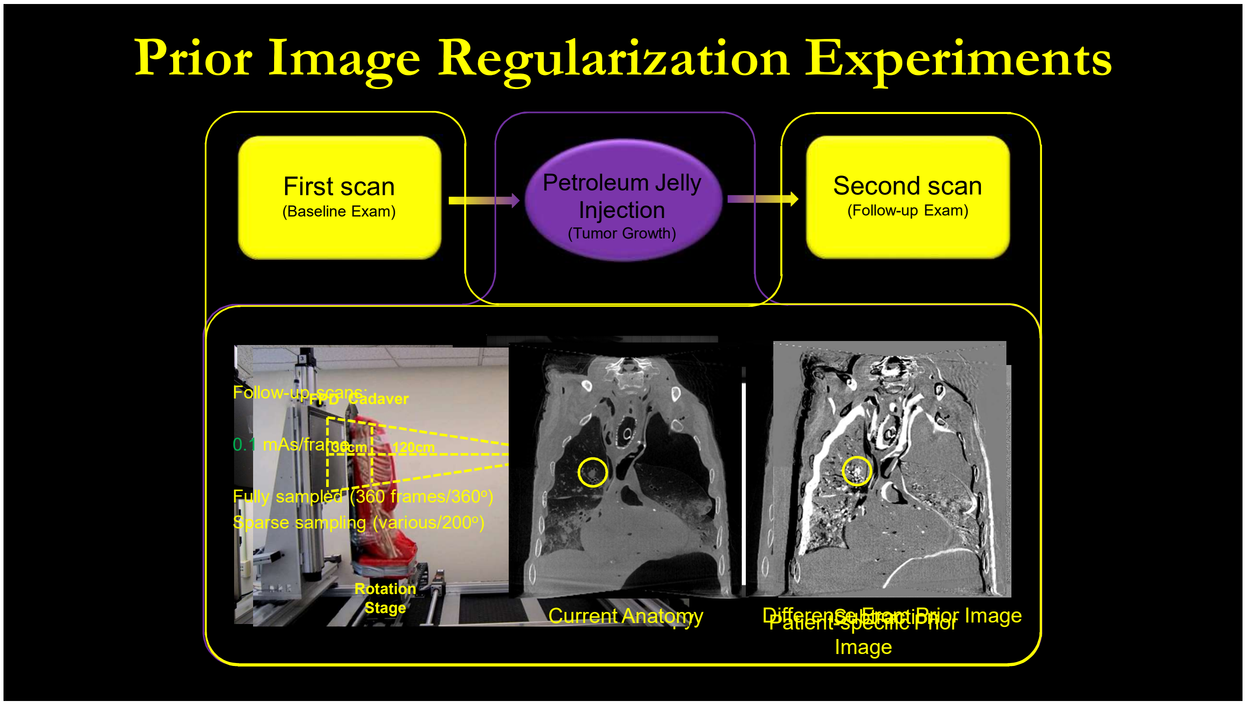
Prior Image Regularization Experiments
First scan
(Baseline Exam)
Petroleum Jelly Injection
(Tumor Growth)
Second scan
(Follow-up Exam)
Follow-up scans:
0.1 mAs/frame
Fully sampled (360 frames/360°)
Sparse sampling (various/200°)
FPD
Cadaver
120cm
Rotation Stage
Current Anatomy
Patient-specific Prior Image

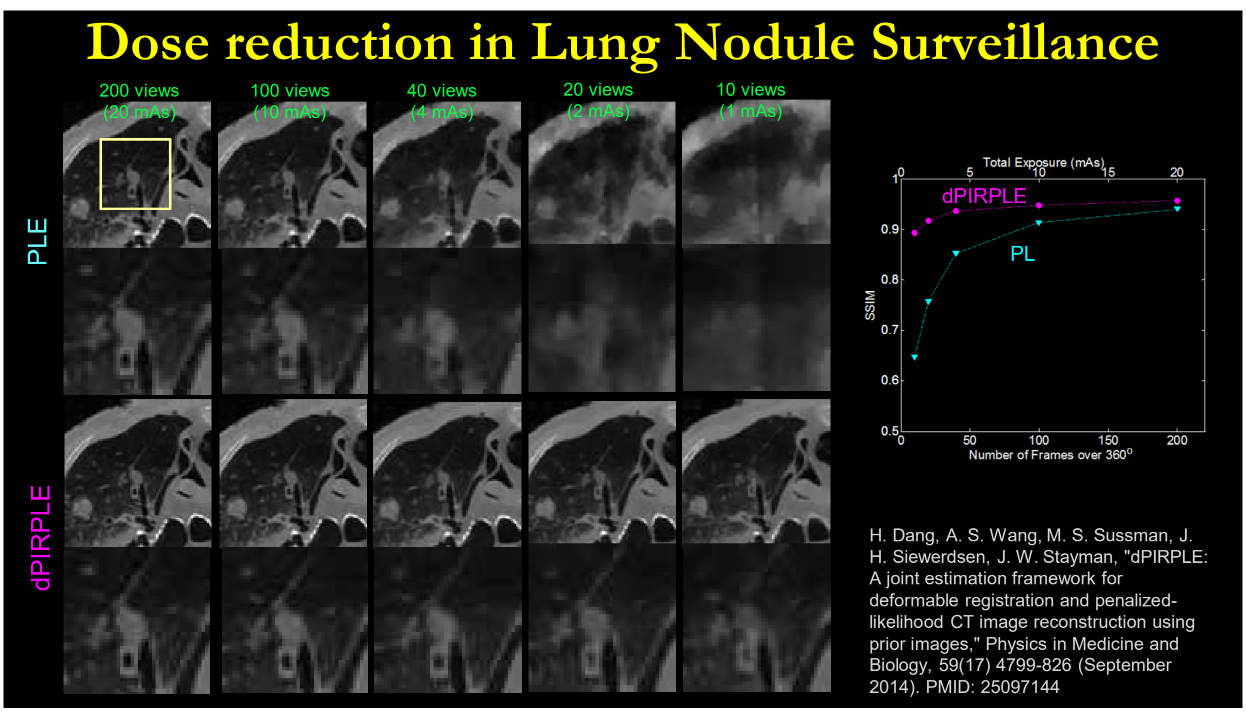
Dose reduction in Lung Nodule Surveillance
200 views
(20 mAs)
100 views
(10 mAs)
40 views
(4 mAs)
20 views
(2 mAs)
10 views
(1 mAs)
PLE
dPIRPLE
Total Exposure (mAs)
0
5
10
15
20
dPIRPLE
PL
SSIM
1
0.9
0.8
0.7
0.6
0.5
0
50
100
150
200
Number of Frames over 360°
H. Dang, A. S. Wang, M. S. Sussman, J. H. Siewerdsen, J. W. Stayman, "dPIRPLE: A joint estimation framework for deformable registration and penalized-likelihood CT image reconstruction using prior images," Physics in Medicine and Biology, 59(17) 4799-826 (September 2014). PMID: 25097144

Prior Images for Image Quality Improvement

Planning MDCT

On-board CBCT Reconstructions

FDK PL PIBR

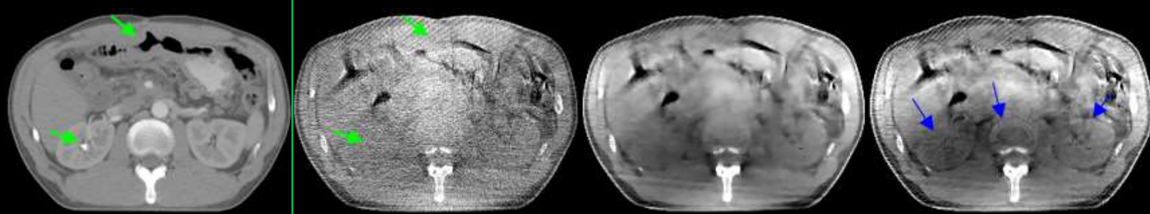

H. Zhang, G. J. Gang, J. Lee. J. Wong, J. W. Stayman, "Integration of prior CT into CBCT reconstruction for improved image quality via reconstruction of difference: first patient studies," Proc. SPIE Medical Imaging Orlando, FL, March 2017, 10132, 1013211-1-6.

Regularization using Patches/Dictionaries

General/learned knowledge of image features

- Need a dictionary of features/patches
- Sparse representations,
  - linear combinations of few patches

Objective Function

$$\{\hat{\mu}, \hat{\lambda}\} = \operatorname{argmax} \log L(y; \mu) - \beta \left(\sum_p \left\| \mathbf{E}_p \mu - \mathbf{D}\lambda_p \right\|_2^2 + \sum_p \nu_p \left\| \lambda_p \right\|_0 \right)$$

D

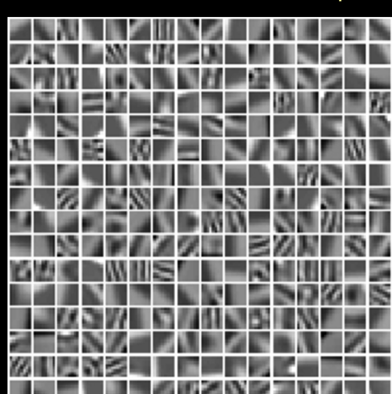

$\mathbf{D}\lambda_p$

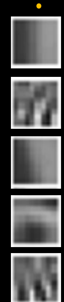

$\mathbf{E}_p \mu$

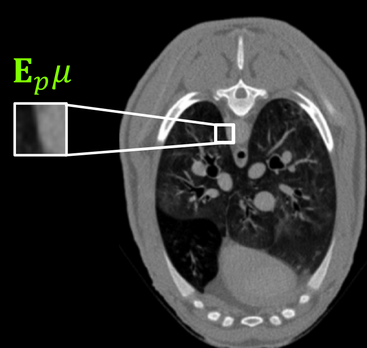

Images adapted from: Q Xu, H Yu, X Mou, L Zhang, J Hsieh, G Wang, "Low-dose x-ray CT reconstruction via dictionary learning," *IEEE Trans. Medical Imaging*, 31(9), September 2012.

Dictionary Methods & Few View Reconstructions

FBP Total Variation Dictionary Methods

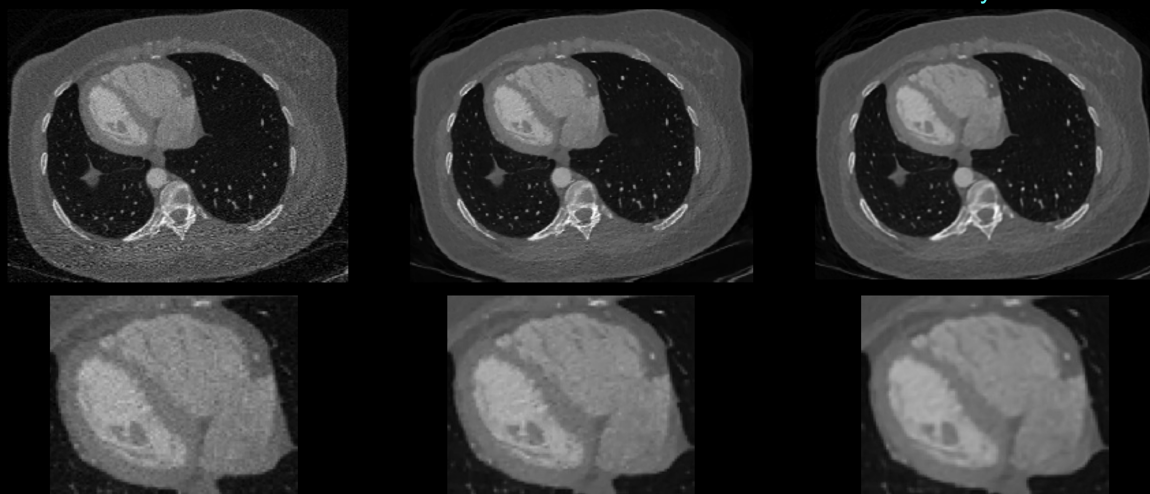

Image credits: Q Xu, H Yu, X Mou, L Zhang, J Hsieh, G Wang, “Low-dose x-ray CT reconstruction via dictionary learning,” *IEEE Trans. Medical Imaging*, 31(9), September 2012.

Additional Information in the Forward Model

$$\bar{y}(\mu) = I_0 \exp(-\mathbf{A}\mu)$$

Forward model has many simplifications in physics…
Model ignores
- Scatter
- Spectral effects
- Focal spot blur
- Detector blur

Object model may have constraints
- Nonnegativity
- Known element/components in the field-of-view

Modeling Known Components in the Object

Implants

- Susceptible to metal artifacts
- Strongest near the device
- Region-of-interest is near implant

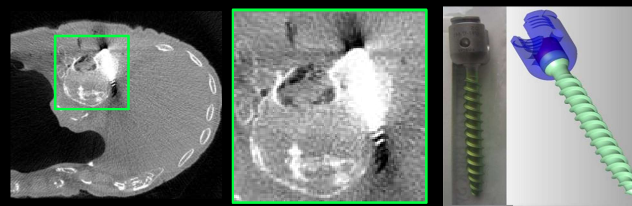

Include a component model in explicitly in the object model

$$\mu(\mu_{\text{anatomy}}, \lambda) = \mathbf{D}\{\mathbf{W}(\lambda)m\}\mu_{\text{anatomy}} + \mathbf{W}(\lambda)\mu_{\text{implant}}$$

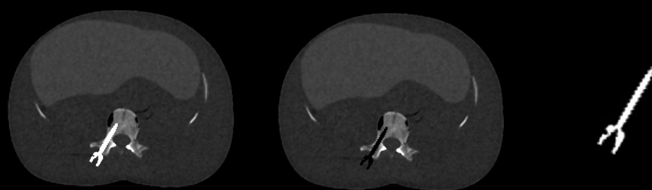

J. W. Stayman, Y. Otake, J. L. Prince, J. H. Siewerdsen, "Model-based Tomographic Reconstruction of Objects containing Known Components," IEEE Trans. Medical Imaging, 31(10), 1837-1848 (October 2012). PMID: 22614574

Known Component Reconstruction Iterations

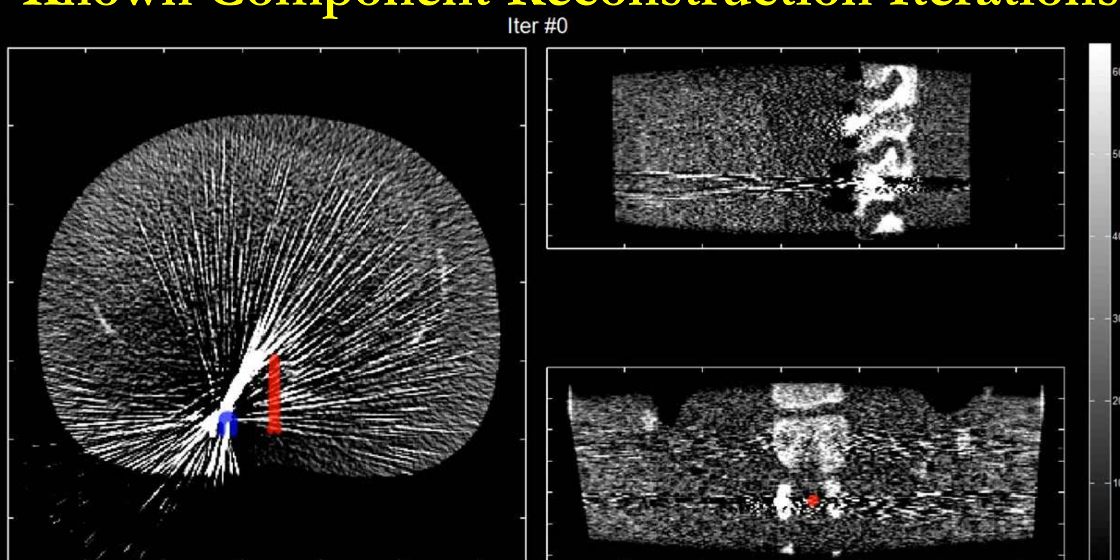

Reconstructions of an Implanted Cadaver

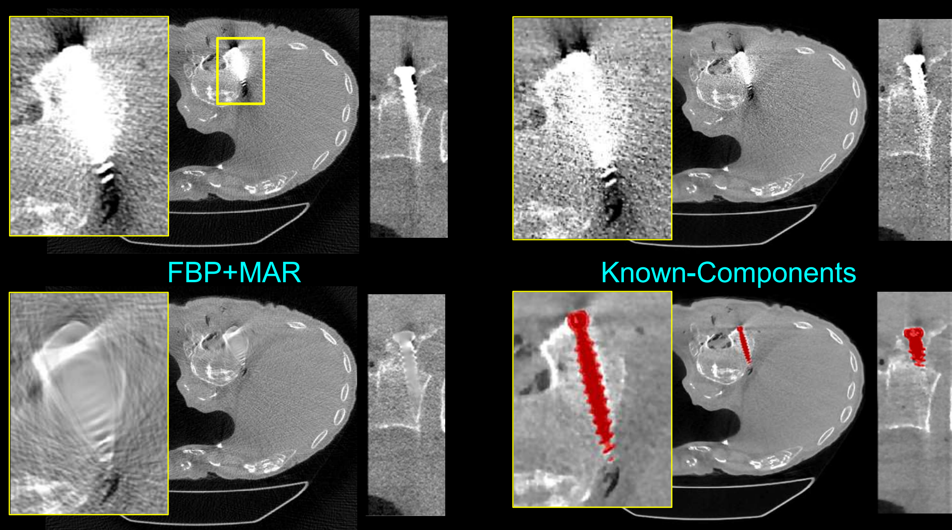

S. Xu, A. Uneri, A. J. Khanna, J. H. Siewerdsen, J. W. Stayman, "Polyenergetic known-component CT reconstruction with unknown material compositions and unknown x-ray spectra," Physics in Medicine and Biology, 62(8), 3352-74 (April 2017)

Improving the Physical Model (Focal Spot Blur)

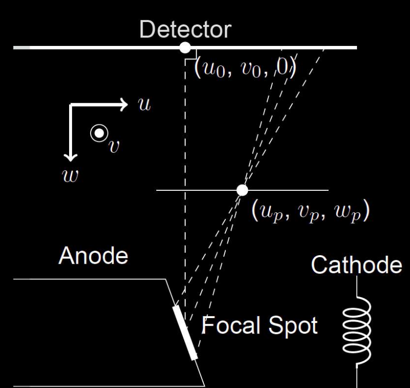

$$\bar{y}_i = \sum_{k=1}^{K} b_{ik} \exp\left(-\sum_{j=1}^{p} a_{kj}\mu_j\right)$$

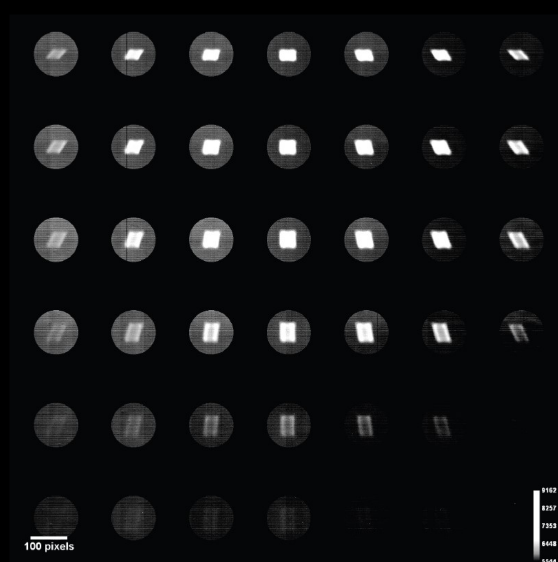

Improved Physical Modeling (Focal Spot)

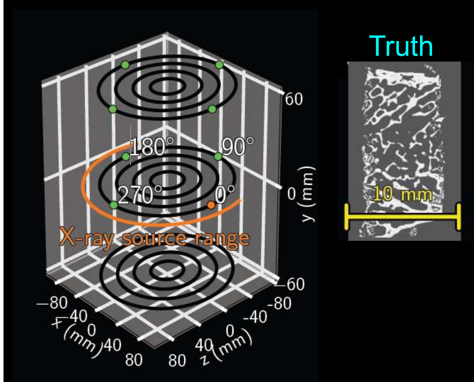

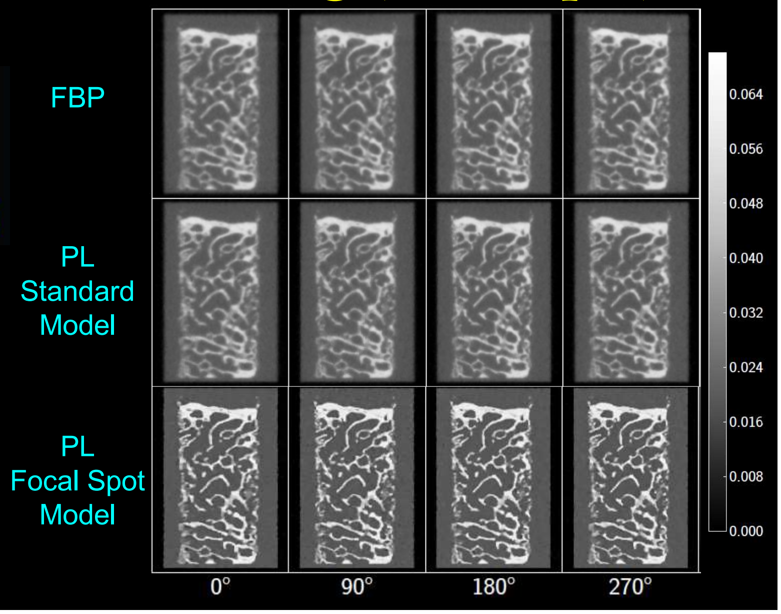

S. Tilley II, W. Zbijewski, and J. W. Stayman, "High-Fidelity Modeling of Shift-Variant Focal-Spot Blur for High-Resolution CT," in *The 14th International Meeting on Fully Three-Dimensional Image Reconstruction in Radiology and Nuclear Medicine*, 2017, pp. 752–759

CT Reconstruction Summary

Advanced Reconstruction Aims
- Dose reduction, improved image quality

CT Forward Model
- Nonlinear, but often linearized
- Measurement statistics are important (SNR varies widely)
- Advanced physical modeling permits image quality improvements

CT Regularization Strategies
- Standard smoothness and edge-preservation
- Use of prior images (e.g., sequential studies)
- Generalized dictionary methods including machine learning

Other Objective Function Modifications
- Additional constraints on the object (e.g., known components)

Acknowledgements

Advanced Imaging Algorithms & Instrumentation Laboratory

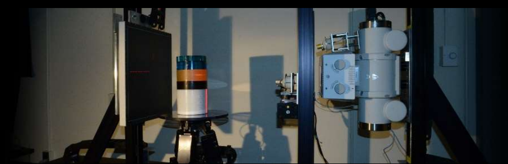

AIAI Laboratory

Advanced Imaging Algorithms and Instrumentation Lab
aiai.jhu.edu
stayman@gmail.com

Faculty and Scientists
Grace Gang (AIAI)
Amir Pormorteza (AIAI)
Jeffrey Siewerdsen (I-STAR)
Alejandro Sisniega (I-STAR)
Adam Wang (I-STAR)
Shiyu Xu (AIAI)
Wojciech Zbijewski (I-STAR)
Hao Zhang (AIAI)

Clinicians
John Carey - Otolaryngology
Kelvin Hong - (Interventional) Radiology
Satomi Kawamoto - Radiology
A Jay Khanna - Orthopaedic Surgery
Eleni Liapi - Radiology
Tony Lin - Radiology
Martin Radvany - (Interventional) Radiology
Marc Sussman - Thoracic Surgery
Clifford Weiss - (Interventional) Radiology
John Wong - Radiation Oncology

Students
Hao Dang
Juliana Carneiro Gomes
Andrew Mao
Gabriela Rodal
Saeed Seyyedi
Steven Tilley II
Ali Uneri
Wenying Wang
Chengzhu Zhang
Esme Zhang

Funding/Support
NIH: U01EB014964, R01EB025470, R21CA219608, R21EB014964, KL2TR001077, R01CA112163
Academic-Industry Partnerships: Siemens, Varian Medical Systems, Elekta AB, Carestream Health
Research Partnership/Agreements: Philips Healthcare, Canon Medical

This work was supported, in part, by the above grants. The contents of this presentation are solely the responsibility of the authors and do not necessarily represent the official view of Johns Hopkins, the NIH, or other organizations.